UNIVERSIDAD NACIONAL AUTÓNOMA DE MÉXICO

INSTITUTO DE ENERGÍAS RENOVABLES

INSTITUTO DE INGENIERÍA

ESCUELA NACIONAL DE ESTUDIOS SUPERIORES-JURIQUILLA

High Dynamic Range photography for daylighting measurements with open technologies

TESIS

Que para obtener el título de

Ingeniera en Energías Renovables

P R E S E N T A

Mariana López Magaña

DIRECTOR DE TESIS

Dr. Guillermo Barrios del Valle

Temixco, Mor., a 6 de octubre de 2021

IER
Instituto de Energías Renovables

INSTITUTO DE INGENIERÍA UNAM

ENES JURIQUILLA

OF/IER/LIER/125/2021
ASUNTO: Notificación de jurado y fecha para examen profesional mediante aula virtual.

LIC. IVONNE RAMÍREZ WENCE
DIRECTORA GENERAL DE ADMINISTRACIÓN ESCOLAR
P r e s e n t e .

Por medio de la presente le informo que el día miércoles 6 de octubre de 2021, a las 10:00 h, mediante Aula Virtual del Instituto de Energías Renovables, habilitada por la Dirección General de Cómputo y de Tecnologías de Información y Comunicación de la UNAM, la **C. MARIANA LÓPEZ MAGAÑA,** con número de cuenta 314093927 de la Licenciatura de Ingeniería en Energías Renovables, llevará a cabo la presentación del trabajo de tesis y examen profesional titulado:

"High Dynamic Range photography for daylighting measurements with open technologies"

Debido a que la alumna ha cumplido con los requisitos que establece el Reglamento General de Exámenes, el Comité Académico de la Licenciatura de Ingeniería en Energías Renovables, le asigna el Jurado de Examen Profesional integrado por los siguientes académicos.

PRESIDENTE:	**DRA. GUADALUPE HUELSZ LESBROS**
VOCAL:	**DRA. ARGELIA BALBUENA ORTEGA**
SECRETARIO:	**DR. GUILLERMO BARRIOS DEL VALLE**
SUPLENTE:	**DR. CAMILO ALBERTO ARANCIBIA BULNES**
SUPLENTE:	**DRA. IRENE MARINCIC LOVRIHA**

Sin otro particular, le envío un cordial saludo.

UNAM
INSTITUTO DE ENERGÍAS RENOVABLES
LICENCIATURA DE INGENIERÍA EN ENERGÍAS RENOVABLES

A t e n t a m e n t e,
"Por mi raza hablará el espíritu"
Temixco, Mor., a 29 de septiembre de 2021

Dr. Jorge Alejandro Wong Loya
Coordinador de la LIER
IER-UNAM

JAWL´mfp.

Priv. Xochicalco s/n,
Col. Centro,
62580 Temixco, Morelos, México
T. 01 (777) 362 00 90
(52) 55 56 22 97 00

ier.unam.mx

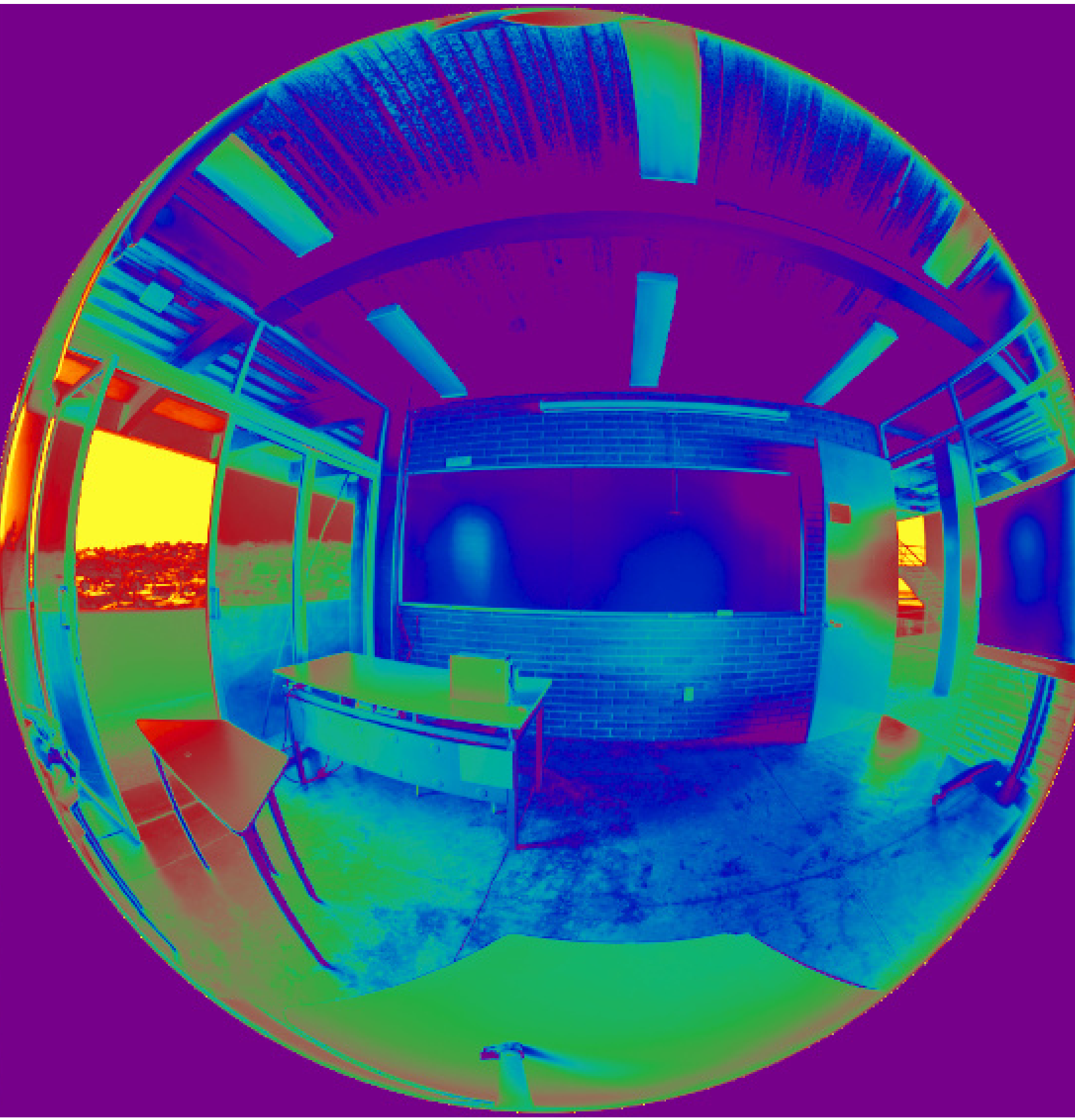

Abstract

The methodology to build a device that can acquire accurate luminance maps from high dynamic range (HDR) images is presented and developed. For this purpose, the calibration of a Canon EOS 6D Mark II camera with an attached fisheye lens is performed in order to generate HDR images. The step-by-step process to calibrate the obtained HDR images and derive luminance maps using the Radiance open software is presented. The process is also automated for a Raspberry Pi with an attached Camera Module V2. Both devices are intended to be used in the new building project of the Renewable Energies Institute of the UNAM "Demonstrative buildings of bioclimatic design in a warm sub-humid climate at the Renewable Energy Institute - UNAM" to evaluate the daylighting conditions inside the building.

Additionally, two experimental campaigns were carried out at the existing spaces of the Renewables Energies Institute of the UNAM. During the first campaign, luminance maps of different spaces were generated and an analysis of the results was carried out to identify possible sources of error during the process. Next, a second experimental campaign was performed, and from the luminance maps obtained, different parameters were analyzed to identify their contribution to the error. From the results, different recommendations are presented to obtain more accurate luminance maps, a luminance analysis was also carried out for some of the spaces, accompanied by an analysis to identify possible glare sources and the calculation of the daylight glare probability (DGP). Finally, conclusions and the areas of opportunity identified during this work are presented. A repository in GitHub that contains the complete files to reproduce the work developed in this thesis is provided.

Dedication

To my parents Gema and Marcos for all their love and support.
To my brother Marcos for always being there for me.
Thank you for giving me wings to fly high.

Acknowledgements

To God, for having the opportunity to live, learn, and experience life.

To Mexico and the UNAM for giving me amazing opportunities to learn and grow in every aspect, and for the scholarships awarded that contributed to my education. To the IER-UNAM, its academic and non-academic staff, and all its community for being my second home during 4 years. Thank you for guiding me through this part of my life, for always being kind, and thank you for the scholarships that supported me along these years.

To the project Demonstration buildings of bioclimatic design in warm sub-humid climate at the UNAM's Renewable Energy Institute (FES-2017-01-291600) sponsored by the Fund CONACYT- Secretariat of Energy-Energy Sustainability 2017-01 Collaboration Projects In Energy Efficiency - Cooperation with the University of California.

Special thanks to my advisor Guillermo Barrios del Valle for his support while developing this work during the COVID-19 pandemic, for trusting me with the equipment, for sharing his knowledge with me and guiding me through this work, for believing in me, for helping me further develop my skills, and for always inspiring me to be better. Also, to Guadalupe Huelsz Lesbros for her valuable contributions, for offering a different perspective at visualizing the results and for letting me collaborate in the project "Demonstrative buildings of bioclimatic design in a warm sub-humid climate at the Renewable Energy Institute - UNAM". To José de Jesús Quiñones Aguilar because his work with the "ESOLMET" allowed me to acquire useful data used in this work. To Wilfrido Rivera Gomez Franco for listening and advising me during my career. To Jesús Muñiz Soria for introducing me to the unknown world of programming. To Ramón Tovar Olvera for his time and knowledge. To Xavier Oscós Vázquez for his support that allowed me to continue. To Maribel, Carlos, Claudia, Magali, Miguel, Paco and Leo for their support and effort. To Clarisa Betancourt for her valuable contributions in different stages of this work. To Kevin Alquicira for keeping alive the Jupyter hub.

To Leticia, Nancy, Gerardo, Clementina, Guadalupe, and all my family that has always been there to cheer me up, and support me in each step of my life. To Ms. Elia, Ms. Maria Luisa and Ms. Bermúdez for all their love and for building the confidence in me along my life. To Sammie and Katy, thank you for the happy moments, a big hug to the sky.

To my roomies Ale and Zyan for being always there, listening and developing my knowledge. To Ray and Georgie for being the best team. To Emilio, Jesús, August, Roy and Rashid for always caring about me. To Caro, Ilse, Jenny and Astrid for their constant support, and for showing me to be strong. To all 6G for being an amazing group and for all the learnings and laughs. To Omar and the 5G for allowing me to learn and sharing part of my journey. To Emeeth for giving me skills for life.

To Gaby, Aldo, Yamil, Bremont, Diana, Lalo, Cris and Liz for being the best friends and always believing in me. To Mitzy, Alan, Diego, Abraham, Julio, Pablo, Leonardo, Leo and Rod for being the best squad, for always taking care of me, and for helping me always see the fun side of life. To Luz, Jiram and Robert, for being amazing friends, for supporting me in every step, and for always bringing joy to my life. To Alondra and Daniela for sharing with me their perspective of life. To Sarah and Tim for keeping my spirit alive during the pandemic, for taking care of me while I was away from home, and for allowing me to be part of their family. To Peter for his wise advise and constant support. To William for letting me be the dreamer. To Alberto for introducing me into the world of architecture. To Luis, Kenyi, Martín, Carlos and Sebastian for sharing good memories with me.

I thank all of the above and all the persons that I have met along my journey, because I have learned from all, and somehow each of them guided me to this stage of my life.

Contents

List of Figures

List of Tables

CHAPTER 1

Introduction

1.1 The importance of light

Humans spend on average 90% of their time indoors [16], and light is an essential requirement to develop most of their activities. Light is fundamental in all aspects of human activities, the non-visual effects of light have begun to be investigated and it has been found that light can affect directly and indirectly people's health. Performing activities under inadequate lighting conditions can lead to a decrement in the productivity of an individual, and mood alterations such as depression. It has been found that light has a great influence on human psychological and physiological behaviors [24].

Both artificial and natural light (the latter also known as daylighting) are usually combined in building design. However, daylighting is nowadays gaining priority, as part of the recommendations from the International Energy Agency (IEA) to increase energy efficiency [2]. Additionally, different studies suggest that daylighting plays an important role to prevent mood disorders, improve sleep quality and alertness, while enhancing the proper functioning of the circadian system, which regulates different body functions including metabolism [4, 30]. However, as daylighting strategies are strongly dependant on season, weather, geographical location, and time of the day among other factors, it is usually combined with artificial lighting to make up for the deficiencies of daylighting. [30].

Designing a healthy and comfortable environment, where lighting needs are satisfied while improving energy efficiency, requires knowing the illumination requirements for the tasks that will be carried out in a space, and the capability to control and adjust different illumination sources, followed by the understanding of the different parameters that influence visual comfort [24]. Usually, the Useful Daylight Illuminance (UDI) index is used to evaluate visual comfort. Glare, which is one of the less understood yet important parameters that has a great influence over lighting comfort can be evaluated using the Daylight Glare Probability (DGP) [6].

Mexico is a privileged country in terms of daylighting. The amount of time that daylighting is available in the country is greater than in countries that are located further away from the equator. Illuminance describes the luminous flux received by unit area. Using weather data from the "Estación solarimétrica y meteorológica of the IER" (ESOLMET-IER) and onebuilding.org, illuminance values along the year for three different cities with different latitudes are created and shown in Figure 1.1, Figure 1.2, and Figure 1.3. Figure 1.1 shows the illuminance values and availability of daylight in Temixco, a city in Mexico, with a latitude of 18.51^o N and a longitude of 99.14^o W, where its maximum illuminance value is 120,000 lx. This map can be compared with the ones shown in Figure 1.2 and Figure 1.3, that show the illuminance values and the availability of daylighting for Fresno, a city in the United States, with a latitude of 36.73^o N and longitude of 119.78^o W, and for the city of Bristol in England, with a latitude of 51.45^o N and a longitude of 2.58^o W respectively. Fresno achieves maximum illuminance of 110,000 lx, while the maximum illuminance for Bristol is near 80,000 lx. From the maps, it is observed that in Temixco, Mexico, high illuminance values are available for long periods of time along the year. Therefore, there is a big area of opportunity to include daylighting into buildings design that can improve visual comfort. For warm climates, a correct lighting design based on diffuse solar radiation can reduce the thermal loads that are generated due to both the artificial lights and the direct solar radiation from the windows, leading to a decrease in the building's energy consumption.

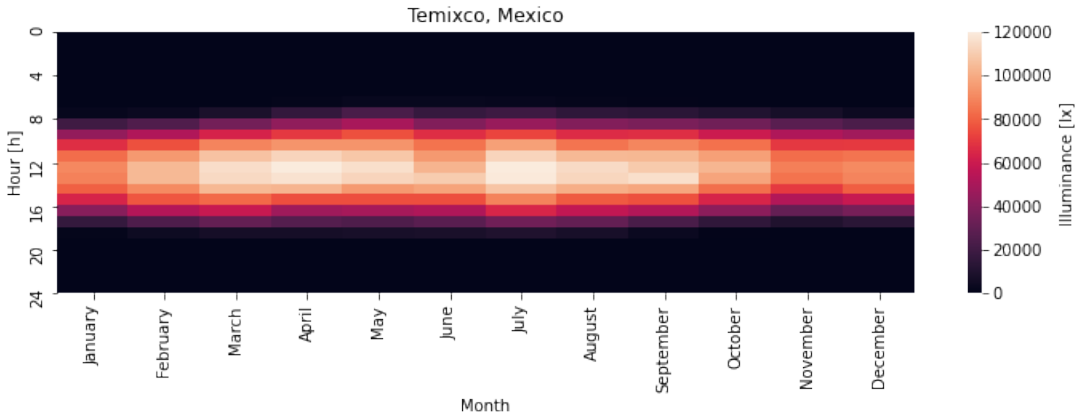

Figure 1.1: Map showing the illuminance values for the city of Temixco with a latitude of 18.51^o N and a longitude of 99.14^o W, for a typical year.

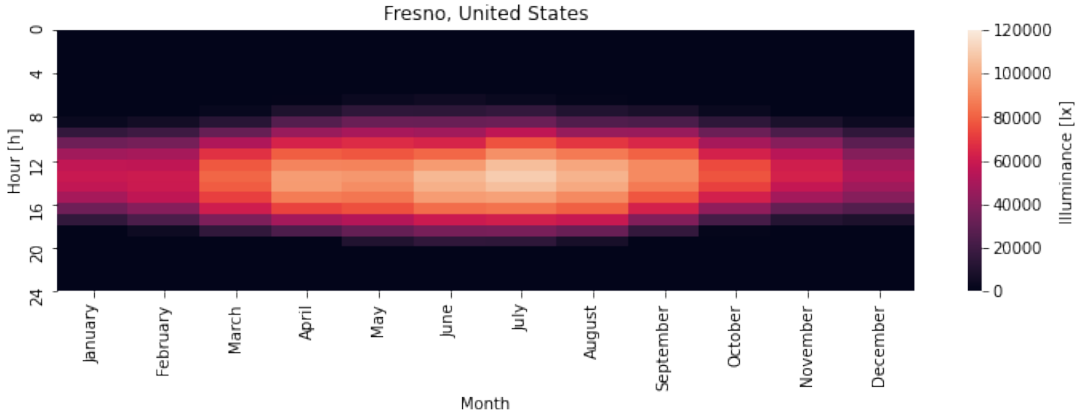

Figure 1.2: Map showing the illuminance values for the city of Fresno with a latitude of 36.73^o N and longitude of 119.78^o W, for a typical year.

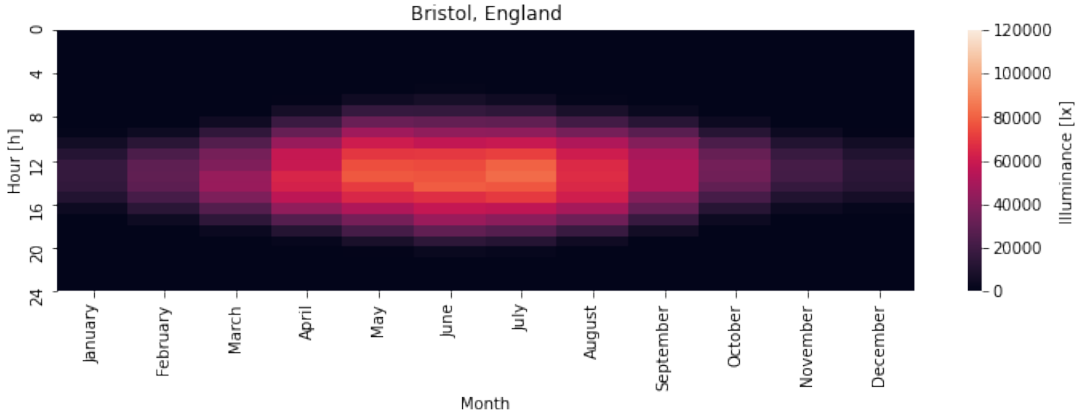

Figure 1.3: Map showing the illuminance values for the city of Bristol with a latitude of 51.45^o N and a longitude of 2.58^o W, for a typical year.

1.2 Luminance maps

Luminance can be described as the luminous flux leaving a surface. In the evaluation of lighting quality, luminance-based metrics are preferred over illuminance ones, as they relate to the human perception of brightness [31]. Part of the tools used to measure lighting quality are luminance maps, as they are able to collect efficiently luminance data within a large field of view, which is not possible to achieve with a luminance meter [13]. Luminance maps are used to evaluate the lighting conditions of different scenarios, as they contain the luminance values of each point of a scene in a particular moment. They can be used to detect glare sources and assess visual comfort, as they show the amount of light that reaches the eyes.

Though high precision luminance cameras are already manufactured and ready to be used for different measuring tasks, they are not widely accessible due to their high price [29]. A more affordable option to acquire luminance maps can be done with a commercially available camera, by taking low dynamic range (LDR) images with different exposure values and merging them to create a high dynamic range (HDR) image. The HDR image has to be then calibrated to obtain a luminance map with acceptable photometric accuracy [22]. During this work, luminance maps are generated and analysed using Radiance, a suite of tools used to perform lighting analyses.

1.3 Objective

The objective of this thesis is to be able to generate accurate luminance maps by performing a step-by-step calibration of two commercially available cameras, a Canon EOS 6D Mark II with a Sigma 8mm f/3.5 EX DG Circular Fisheye Lens and a Raspberry Pi with a Camera Module V2 with an attached MakerFocus fisheye lens. Fisheye lenses are preferred during this work because of their 180 ^{o} field of view, which allows to analyze a wider part of a scene. Both cameras are intended to be used in the new building project of the Renewable Energies Institute of the UNAM "Demonstrative buildings of bioclimatic design in a warm sub-humid climate at the Renewable Energy Institute - UNAM" to evaluate the lighting conditions within the building. The Canon camera is aimed to be utilized in experimental campaigns, where the derived luminance maps can be used to evaluate the illumination in the scene, identify possible glare sources and calculate glare metrics. Conversely, the Raspberry Pi Camera is planned for continuous long-term acquisition of luminance values in all classrooms, due to its low price. However, no glare analysis is intended to be done with the maps obtained from the Raspberry Pi, as it is intended to be positioned away from the occupants sightline.

The Radiance suite is used to merge and calibrate the HDR images with a point-in-time illuminance measurement as reference, as well as making the glare analysis. Problems encountered during the HDR image calibration are addressed and suggestions to enhance the accuracy of the luminance maps are presented. Finally, the scripts of the automated process to acquire luminance maps for both cameras are included in the appendices.

CHAPTER 2

Theoretical background

2.1 Radiometry and photometry

Radiometry is the measurement of radiation from all wavelengths and describes the energy transfer from a source to a detector. Radiance (P) and irradiance (I) are its basic concepts where the former refers to the radiant flux per unit solid angle measured in $[\frac{W}{m^2 sr}]$, and the latter is the density of radiant flux per unit area measured in $[\frac{W}{m^2}]$. Photometry measures light or radiation in the visible spectrum based on the response of the human eye, where luminance (L) and illuminance (E) are the counterparts of the basic radiometric variables weighted in the visible spectrum. Luminance, therefore, is defined as the luminous flux leaving (i.e. emitted, reflected or transmitted) a surface measured in $[\frac{lm}{m^2 sr}]$ or $[\frac{cd}{m^2}]$, and illuminance as the luminous flux received by unit area measured in $[\frac{lm}{m^2}]$ or $[lx]$. In this thesis $[\frac{cd}{m2}]$ and $[lx]$ are used.

2.2 Light

Visible light can be described as the part of the electromagnetic radiation perceived by the human eye, which is produced by moving charged particles that create fluctuations in the magnetic and electric field. Electromagnetic radiation carries energy in the form of electromagnetic waves. These waves have different wavelengths and make up the electromagnetic spectrum, shown in Figure 2.1.

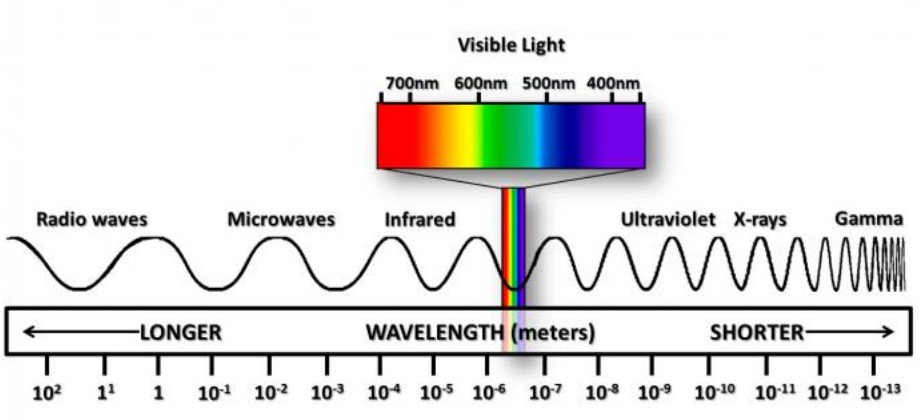

Figure 2.1: The electromagnetic spectrum and the range of electromagnetic radiation perceived by the human eye [18].

2.2.1 Luminosity function

The human eyes can detect wavelengths ranging from 380 to 780 nm thanks to special cells called cones and rods, which are used depending on the lighting conditions. Vision can be classified into photopic, scotopic and mesopic: Photopic vision dominates under well-lighted conditions, where three different types of cones sensible to short,

middle, and long wavelengths are used to mediate the perception of color. In darker scenes scotopic vision dominates, where rods, despite being insensitive to different colors, exhibit a higher sensitivity to light. Mesopic vision uses both, cones and rods at the same time, and it is the kind of vision human eyes use most of the time [1].

However, cones and rods are not equally sensitive to the different wavelengths. To describe the spectral sensitivity of the human eyes to different wavelengths, luminosity functions have been derived for photopic, scotopic and mesopic vision. In Figure 2.2, the luminosity functions for scotopic, mesopic and photopic vision are shown, where the luminous efficiency represents the standardized brightness of different wavelengths as perceived by the human eye [9]. The photopic vision reaches its maximum at 555 nm, and the scotopic vision reaches its maximum at 507 nm.

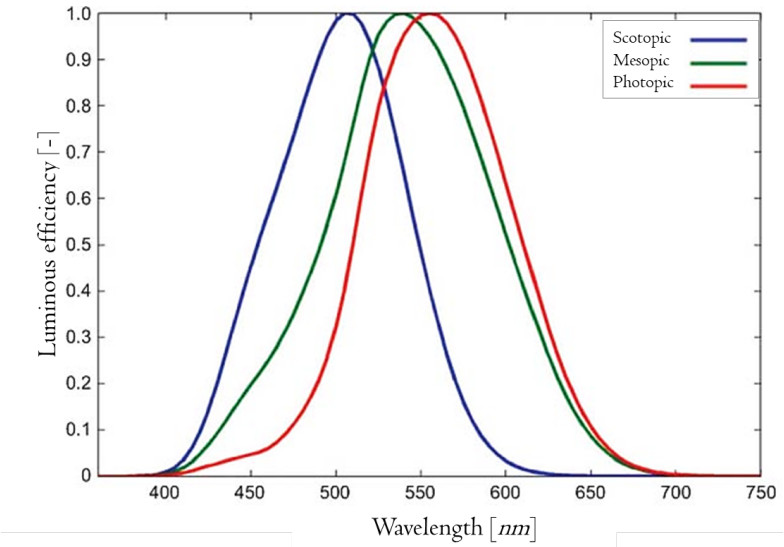

Figure 2.2: Luminosity function for the scotopic, mesopic and photopic vision [9].

2.3 Glare

Glare can be described as the visual sensation caused by excessive brightness in the field of view and it is usually classified into disability and discomfort glare. Disability glare occurs when having a very bright light source in the field of view, which produces light scattering in the eye, disabling the eye to produce a correct image. Discomfort glare is defined by the International Commission on Illumination (CIE) as the visual conditions that due to their excessive contrast, or the inappropriate distribution of light sources, disturbs the observer or limits the ability to distinguish details and objects. [17].

Different methods to evaluate glare have been proposed, where the luminance of the glare source, the solid angle subtended by the source, the angular displacement of the glare source from the subject sightline, and the background luminance are the parameters considered in most models. A reliable glare prediction model proposed by Wienold is the Daylight Glare Probability (DGP) [27], which describes the probability of a person being disturbed by the glare, instead of the glare magnitude. The model takes into account from $i = 1$ to n glare sources present in a scene, and is described by the following equation:

$$DGP = 5.87 \times 10^{-5} E_v + 9.18 \times 10^{-2} log\left(\sum_{i}^{n} \frac{L_{s,i}^2 w_{s,i}}{E_v^{1.87} P_i^2}\right) + 0.16, \tag{2.1}$$

where E_v is the vertical eye illuminance $[lx]$, $L_{s,i}$ is the luminance of the ith source $[\frac{cd}{m^2}]$, $\omega_{s,i}$ is the solid angle of the ith source, P_i is the position index of the ith which indicates the amount of discomfort a glare source produces depending in its angular displacement from the observer's line of sight [27].

The illuminance of a scene is measured with an illuminance meter. Then, the glare perception of the subject can be identified according to the DGP value as shown in Table 2.1. It should be noted that the DGP is only valid for values between 0.2 and 0.8, and when the vertical illuminance is greater than 380 lx [27].

Glare perception	DGP
Imperceptible	≤ 0.352
Noticeable	≤ 0.394
Disturbing	≤ 0.456
Intolerable	≤ 0.590

Table 2.1: Glare ratings according to the DGP value [26].

2.4 Digital Photography

Digital cameras work similarly to the human eyes. Lenses, which are the camera's optical components make incident light converge into an electronic sensor in charge of processing the information and creating the digital image [5]. Camera lenses are made up of a series of concave and convex crystals that focus light to strike the camera sensor in the correct way. Camera sensors are made up of several pixels that measure light intensity. Every time a photon strikes a pixel, a voltage difference is recorded by the sensor to recreate the image. In order for the color to be perceived, a Bayer filter, shown in Figure 2.3, is attached on top of the sensor, which helps to detect wavelengths corresponding to red, green and blue colors which are then combined to obtain a wider range of colors, depending on the number of bits of the camera. Each pixel in a color image has pixel channels, which correspond to the primary colors that make up the image i.e red, green and blue (RGB) colors. Each of these channels correspond to 8 bits, giving a total of 255 possible values for each channel. Then, a pixel with RGB values equal to zero, i.e (0,0,0) is black color, whereas a pixel with RGB values equal to 255, i.e.(255,255,255) is white.

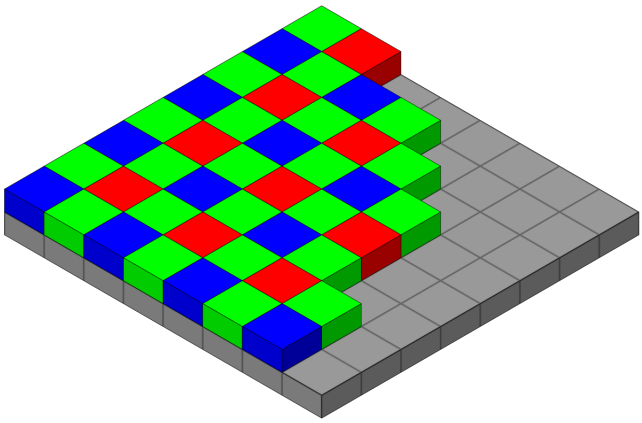

Figure 2.3: Bayer filter [28].

2.4.1 Exposure value

The exposure value (EV) represents the amount of light that reaches the camera sensor [10], and determines how bright or dark a picture appears. The exposure value of an image is defined by the combination of three camera settings: ISO, shutter speed and lens aperture.

ISO is the value that determines how sensible is the camera sensor to the incoming light. Higher ISO values amplify the output digital signal produced by the photons when striking the camera sensor, therefore less light is needed to produce a brighter image as long as shutter speed and aperture remain constant. However, it is recommended to increase ISO values just in cases where shutter speed or lens aperture values are not enough to obtain the desired exposure, as digital signals produce noise, which increases when amplified, decreasing the sharpness of the image [20]. Aperture refers to the opening of a lens diaphragm through which light passes to reach the sensor, and is measured in f/stops. An f/stop is equivalent to the f/number, which describes the ratio between the lens focal length and the diameter of the diaphragm opening. The lower the f-number the more light is allowed into the camera and conversely. Shutter speed defines the amount of time the shutter will be opened, letting light

enter through the lens and reach the sensor. A high shutter speed is able to freeze motion, while a long shutter speed records more light into the sensor and may create a blurring effect for moving objects [5]. Additionally, an EV value stop refers to doubling or halving the amount of light that reaches the camera sensor. The EV value of an image can be increased or decreased either by changing the aperture, i.e, aperture stop, changing the shutter speed, i.e, shutter speed stop, changing the ISO value, i.e, ISO stop, or a combination of the three.

2.4.2 Image file format

The most common file formats in which digital cameras store their pictures are RAW and JPEG. RAW format contains unprocessed data from the digital camera's sensor, which can be retrieved after processing the picture with a raw converter. Having the unprocessed data allows RAW pictures to yield a greater dynamic range, however as it is a lossless compression, RAW images occupy more memory storage. JPEG file format requires much less memory storage than RAW pictures, and it is processed directly on the camera to output a compressed picture. However, by compressing the information to output a JPEG image file, some data of the sensor is lost and cannot be later recovered.

The camera's response function relates the flux of energy emitted by the scene, to the flux received by each pixel of the image (i.e. scene radiance and image brightness respectively) [12]. Although both JPEG and RAW formats can preserve luminance data [22], in RAW images, the camera's response function is stored, whereas in JPEG formats this information is lost. Therefore, RAW formats are used during this work.

2.4.3 HDR images

HDR stands for "High Dynamic Range", where dynamic range refers to the ratio between the brightest and darkest spots of a scene, and is measured with exposure value stops (EV stops). An increase of 1 EV stop will double the amount of light of the image, whereas a decrease of 1 EV stop will half the amount of light of the image. Human eyes are able to achieve a dynamic range of 10 to 14 EV stops, whereas professional cameras are limited to a dynamic range of 8 to 11 EV stops [19]. Despite cameras capturing low dynamic range (LDR) images, HDR images can be achieved by capturing multiple LDR images with different EV values from the same scene and merging them together. HDR images contain the relative luminance values of a scene, for a HDR image to show the real luminance values of a scene to be able to be used as a luminance map, a photometric calibration needs to be done. A photometric calibration converts the relative luminance values of an image to absolute luminance values, by using a luminance measurement of a part in the scene as a reference point.

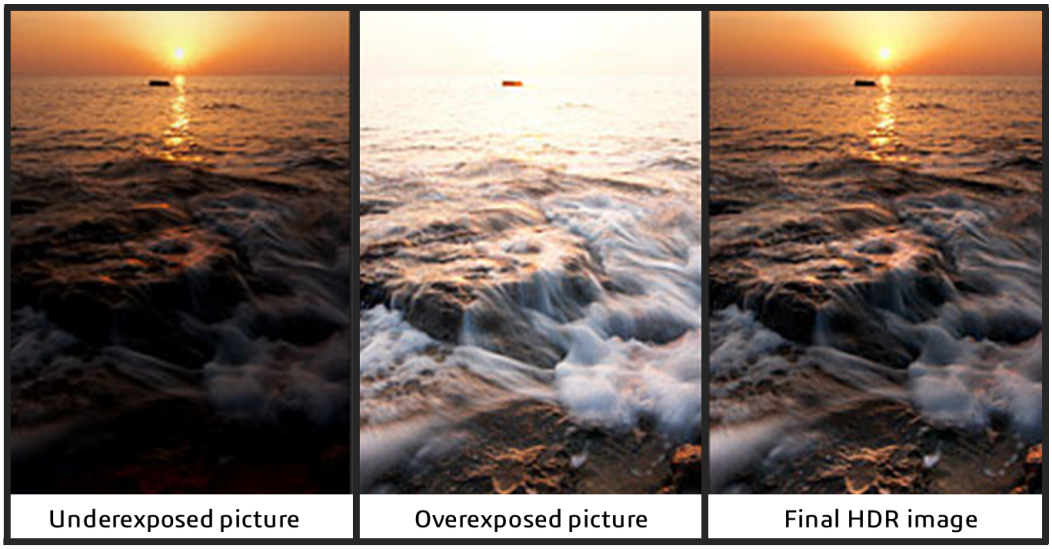

Figure 2.4: Example of a high dynamic range (HDR) image composed from two low dynamic range (LDR) images, one underexposed and one overexposed [19].

CHAPTER 3

Calibrations and experimental setup

Before taking a set of low dynamic range images (LDR) and combining them to create a high dynamic range image (HDR), the camera lens and sensor need to be calibrated to ensure that they are in optimal conditions . Therefore, in this chapter, the process required to calibrate the camera and the fisheye lens is presented in section 3.1. First, the process to identify damaged pixels is presented. Next, the methodology to find the non-parallax point of the fisheye lens is described, followed by the procedure to determine the fisheye real angle of view. Then, the vignetting effect in lenses is explained, along with the most common method to determine the vignetting curves of a fisheye lens with different apertures. The importance of conducting these calibrations is discussed in each step and the results are shown. Finally in section 3.2 the setup used during this work is shown. The hardware and software used during this thesis to acquire luminance maps are listed in Appendix A.

3.1 Camera sensor and lens calibration

3.1.1 Finding damaged pixels

Filters made up of red, green and blue (RGB) colors are called Bayer filters, where each different color filters the light of its corresponding color ignoring the rest. At the end, the information of the red, green and blue filters is gathered to display the actual color in what it is called an RGB image.

However, some pixels in the sensor might be damaged, meaning that they will show wrong measurements of the incident light falling on them. These pixels can be classified as dead, stuck, or hot pixels. Dead pixels do not produce any signal and therefore will look black as they are not recording any light value, conversely, stuck pixels record always the same information about the received light and will tend to keep the same color among several pictures [22]. Hot pixels are caused by a charge leakage due to a temperature increase in the sensor, and therefore are more likely to appear under long exposures. As the color filter is neglected, hot pixels look completely white.

In order to identify dead pixels, taking pictures of non-black scenarios is recommended, avoiding long exposures as this might cause hot pixels. All the black pixels identified in the image are likely to be dead pixels. On the other hand, stuck pixels and hot pixels can be identified by taking several pictures with the lens cap on and different time exposure, where stuck and hot pixels will appear colored or white in the image.

Additionally, when taking a picture random variation of brightness or color can happen. This is called image noise. In photography, the most common types of image noise produced when taking a picture are called Gaussian and Poisson noises. The former can be produced due to poor illumination in the scene, high temperatures, or the electronics within the sensor, and is randomly distributed over the entire image, while the latter is a result of light natural fluctuation [8].

The camera used in this work is a Canon EOS 6D Mark II, which has a sensor resolution of 26 MP. It is important to check for dead, stuck and hot pixels since a great number of damaged pixels (i.e more than 1% of the total amount of pixels) could result in distorted measurements, hence camera should be changed.

When checking for dead, stuck or hot pixels in the camera sensor, the lens is not attached to the camera as the electronics in it are likely to increase the noise in the images due to the heat produced by it. To find if there are any dead pixels, the camera's lens mount is uncovered and one image is taken under a short exposure and low ISO value. Then the image is visualized in RawTherapee (an open RAW image editor) for a qualitative inspection of the pictures.

Figure 3.1 shows the image taken and visualized in RawTherapee. The image is then processed in Python using rawpy to make a quantitative inspection. Rawpy is a Python wrapper for the LibRaw library which allows to process RAW images and handle the data contained in the array of pixels. The RGB values of each pixel of an image are represented in a 3D matrix. In order to identify the dead pixels, a code is made to count the amount of pixels that have their RGB values simultaneously equal to zero. For this work, the code is written in Python as follows:

```
dead = rawpy.imread('Image.CR2')
dead = dead.postprocess()
count_raw=dead.sum(axis=2)
count=count_raw.reshape(4180,6264,1)
raw_true=((count[:,:]==0))
np.count_nonzero(raw_true)
```

In the particular case of Figure 3.1 no dead pixels were detected, therefore the camera sensor has no dead pixels.

Figure 3.1: Image where camera settings are: ISO 100 and 1/50s of exposure time.

To check for stuck and hot pixels, the camera lens mount is covered with the cap and a series of ten pictures, varying exposure time and with ISO set to 100, are taken. An ISO value of 100 is selected in order to minimize the noise in the image. Figure 3.2 shows IMG1 with a 1600% zoom visualized in RawTherapee, and Table 3.1 shows the settings for each picture taken.

Image[-]	IMG1	IMG2	IMG3	IMG4	IMG5	IMG6	IMG7	IMG8	IMG9	IMG10
ISO [-]	100	100	100	100	100	100	100	100	100	100
Exposure time [s]	30	1/4000	1/1000	15	8	1/100	1/10	5	2	1

Table 3.1: Settings of the pictures taken with the lens mount cap on and in RAW format.

The colored pixels in Figure 3.2 correspond to Gaussian noise produced by the electronics in the camera sensor. Noise from the image has to be removed in order to correctly identify the pixels that are truly damaged, then the remaining white and colored pixels are likely to be stuck or hot pixels respectively.

Denoising of the image and detection of stuck and hot pixels is done with Python using rawpy library, where the set of 10 images with different exposure values previously taken are provided. As noise has a random behavior, pixels among the different images are compared and only those that appear colored in the different images will be identified as stuck or hot pixels. In rawpy, the similar nature of stuck and hot pixels encloses them in the same concept (i.e. find_hot), and a confirmation ratio is assigned to the process to set the number of images that should have the same colored pixel for it to be consider as damaged.

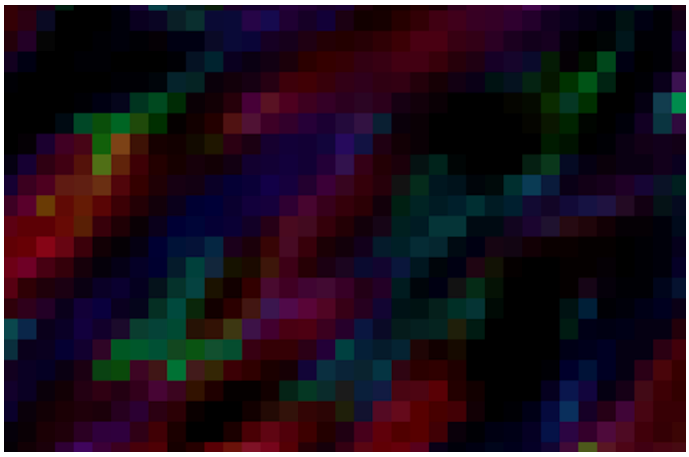

Figure 3.2: IMG1 with a 1600% zoom, where camera settings are: ISO 100 and 30 s of exposure time (The brightness of the image is increased to highlight the colors).

To read, denoise, and identify stuck and hot pixels from a set of raw images, rawpy library in Python is used as follows:

```
paths=['IMG1.CR2', 'IMG2.CR2', 'IMG3.CR2', ..., 'IMG10.CR2']
bad_pixels = rawpy.enhance.find_bad_pixels(paths,find_hot=True, confirm_ratio=0.9)
```

For the Canon EOS 6D Mark II, just one damaged pixel (i.e either stuck or hot) is found. Then, in order to confirm the result, 10 additional images are taken with the lens mount cap on and different exposure time values. The settings of this additional set of images are shown in Table 3.2, and are added one by one to the previous set of images, where no additional hot or stuck pixels are found.

Image[-]	IMG11	IMG12	IMG13	IMG14	IMG15	IMG16	IMG17	IMG18	IMG19	IMG20
ISO [-]	100	100	100	100	100	100	100	100	100	100
Exposure time [s]	8	4	2	1/2	1/4	1/6	1/8	1/15	1/30	1/60

Table 3.2: Settings of the second set of pictures taken with the lens cap on and in RAW format.

The damaged pixel found in the sensor is plotted in Figure 3.3, whose coordinates [x,y] are:

```
[1586, 3633]
```

Because no dead pixels are found in the sensor, and only 1 out of 26 megapixels is found to be hot or stuck, it is concluded that the camera's sensor is in optimal conditions to be used during this work.

3.1.2 Fisheye real angle of view

Lenses bend light and focus it over the camera sensor. Light rays entering the lens have different directions, from which we can define marginal and chief rays. Marginal rays are the ones that have their origin in the optical axis and pass at the maximum aperture of the lens, while chief rays have their origin from an off axis point and pass through the center of the aperture stop [15], a diagram representing these definitions is shown in Figure 3.4.

The entrance pupil of a lens is the plane where virtual chief rays would intersect the optical axis. The center of the entrance pupil otherwise referred to as the "non-parallax point" is the vertex of the lens angle of view. It is important to identify the non-parallax point of the lens to know the point where all the light rays converge, as this will be the reference point to calculate the real angle of view of the lens. Additionally, rotating the camera around this point will avoid parallax error, which refers to the apparent displacement on the position of an object.

The lens angle of view is measured in degrees and corresponds to the angle between objects on opposite borders of the lens. Fisheye photographic lenses have a wide angle of view, they are designed to see up to 180°, however the

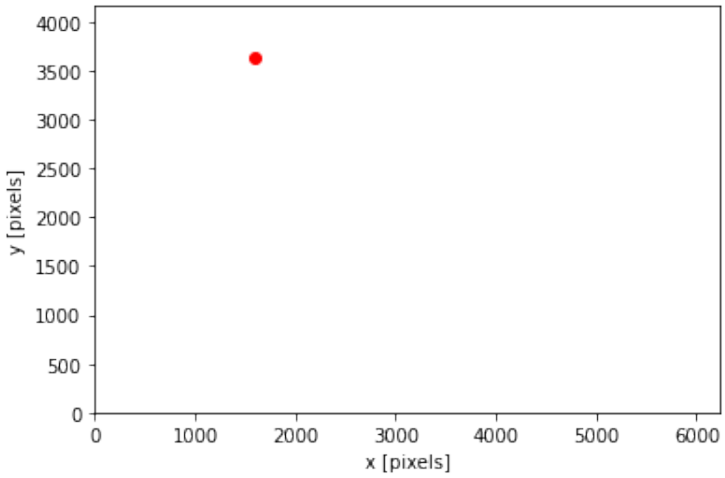

Figure 3.3: Plot showing the position of the damaged pixel found in the camera sensor.

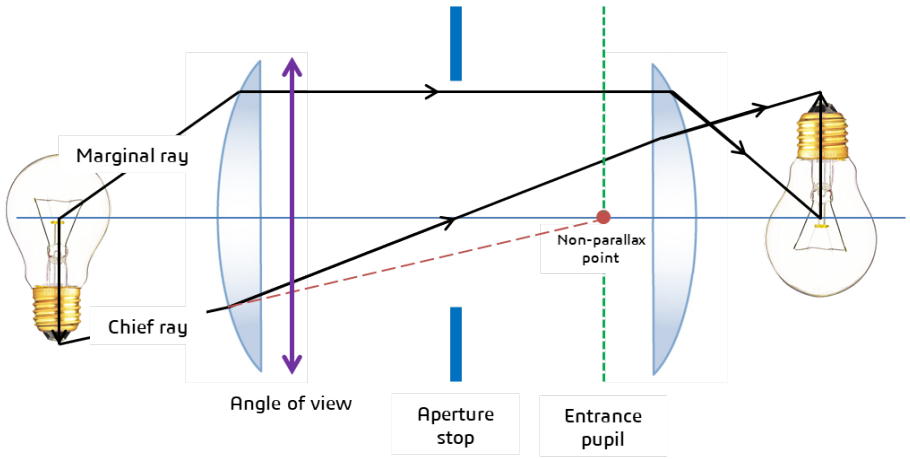

Figure 3.4: Marginal and chief rays diagram, (adapted from [15]).

real angle of view could be a couple degrees more or less depending on the lens. Knowing the real angle of view of a fisheye lens is important to correctly determine the solid angle and position of different glare sources in the scene [22].

3.1.3 Finding the entrance pupil

Unlike common lenses, fisheye lenses do not have a single location for the entrance pupil, in fact, the entrance pupil of the lens moves along the optical axis due to the spherical aberration [25]. Therefore in these type of lenses there is not a single "non-parallax point", but rather different least-parallax points. Then, the mid least-parallax point should be selected and considered the non-parallax point of the lens. As the rays converge there, panning the camera around this point will avoid parallax error [22].

In order to find the lens least-parallax point, two vertical objects are aligned at a distance of 0.5m from each other, as shown in Figure 3.5. Then the camera is positioned one meter away from the first vertical object, set up on a nodal rail as shown in Figure 3.6, attached to a tripod, facing and aligned with the vertical objects. The complete setup is illustrated in Figure 3.7.

Taking a picture with the described set up shown in Figure 3.7 will make the two vertical objects look as one when facing them. Panning the camera from left to right around the least-parallax point of the lens would make the two objects still look as one, however if that is not the case, then, panning to either side will make the last object

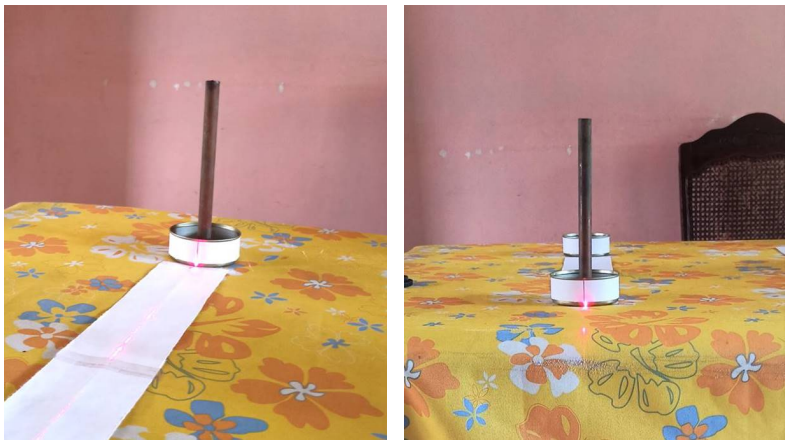

(a) Further vertical object alignment. (b) First vertical object alignment.

Figure 3.5: Alignment of the two vertical objects separated 0.5 m from each other.

(a) Camera placed on nodal rail.

(b) Camera displaced along the nodal rail.

Figure 3.6: Movement of the camera along the nodal rail to find the least-parallax point.

visible in the picture as shown on Figure 3.8.

To find the least-parallax point the camera should be slid along the nodal rail and then panned right and left, until finding the point around which the last vertical object is no longer seen, as in Figure 3.9.

Following the procedure described, and taking as reference the golden ring of the fisheye lens, the least-parallax point of the Sigma 8mm f3.5 fisheye lens is found to be 3 mm behind the golden ring.

3.1.4 Real angle of view

Being the least parallax point the vertex of the lens angle of view, the assumption can be made that a half circle (i.e. 180°) whose center is the least parallax point of the lens as shown in Figure 3.10, should be completely seen by the fisheye lens. If that is not the case, then the fisheye would be seeing more or less than 180°. The setup drawn in Figure 3.10 is used to determine the camera real angle of view.

To find the real angle of view of the fisheye lens the following steps are followed:

1. A laser is fixed on a horizontal surface, and projected into a vertical surface one meter away.

2. The laser projection is marked on the vertical surface.

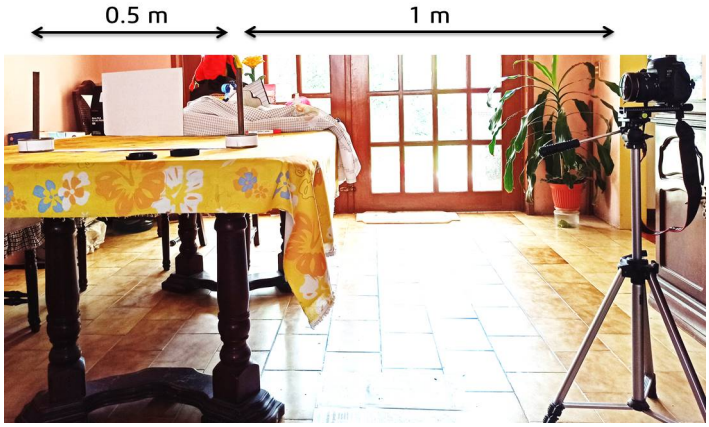

Figure 3.7: Setup for finding the least-parallax point.

(a) Camera panned left. (b) Camera on the center. (c) Camera panned right.

Figure 3.8: Camera panned around the point located 10 mm behind the lens golden ring.

(a) Camera panned left. (b) Camera on the center. (c) Camera panned right.

Figure 3.9: Camera panned around the point located 3mm behind the lens golden ring, in the least-parallax point.

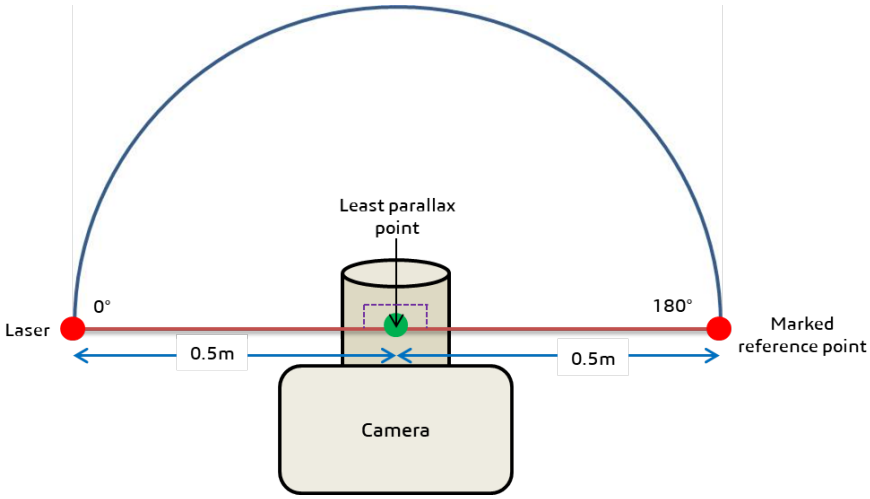

Figure 3.10: Aerial scheme of the set up to determine real angle of view.

3. The midpoint of the line between the laser and the mark on the vertical surface is located. The midpoint corresponds to the center of a circle on the horizontal surface with one meter diameter.

4. At five degree intervals, radial lines are drawn from the center of the circle to the perimeter, and extended into a vertical surface, as shown in Figure 3.11.

5. After drawing the lines in the vertical surface, the camera lens least-parallax point will be aligned with the center of the circle. The camera lens should be perpendicular to the laser and the marked reference point as shown in Figure 3.10.

6. In this position a picture is taken with the camera.

7. The real angle of view of the lens is calculated using the laser and marked reference point.

If the fisheye lens had an angle of view of 180°, taking a picture with the camera in the position as shown in Figure 3.12 would show the laser and the reference point at the opposite borders of the image. However, when this is done, additional pixels from each side can be seen in the image, which means the real angle of view of the lens is greater than 180°. The picture taken by the camera is displayed in Figure 3.13.

The image is opened in RawTherapee and because the lens has an equidistant projection, to determine how much more the camera lens is seeing a 1:1 100% zoom is made and the number of pixels between two of the lines drawn each 5 degrees before, are counted and a pixel-angle relationship is derived. Then the additional number of pixels shown in the picture are counted for each side, and using the pixel-angle relationship, the real angle of view is obtained. In Figure 3.14a and Figure 3.14b a 1:1 100% zoom is shown on both opposite borders of the image.

The complete procedure is replicated 3 times. From them, the pixel-angle relationship where 8 pixels at a 1:1 100% zoom account for 5° is derived, and the average real angle of view is found to be 185° ± 0.5°, which is similar to the one reported in [22], which was 186° for the same lens.

3.1.5 Vignetting

In optical systems the decrease in brightness of an image relative to its center is called the vignetting effect. Vignetting increases with fisheye lenses and it is a function of the lens aperture, where small apertures increase the vignetting effect while bigger apertures reduce it [22].

Vignetting in pictures can be corrected by deriving a vignetting curve. A vignetting curve defines the vignetting factor that should be applied to each pixel according to its position [22]. The most common method for deriving this curve requires a non-flickering, constant and uniform target placed in front of the camera. The camera is rotated every five degrees around its non-parallax point and in each step a sequence of pictures varying exposure is taken. Then, an HDR image is created for each step and the luminance value of the target is derived from it. The vignetting

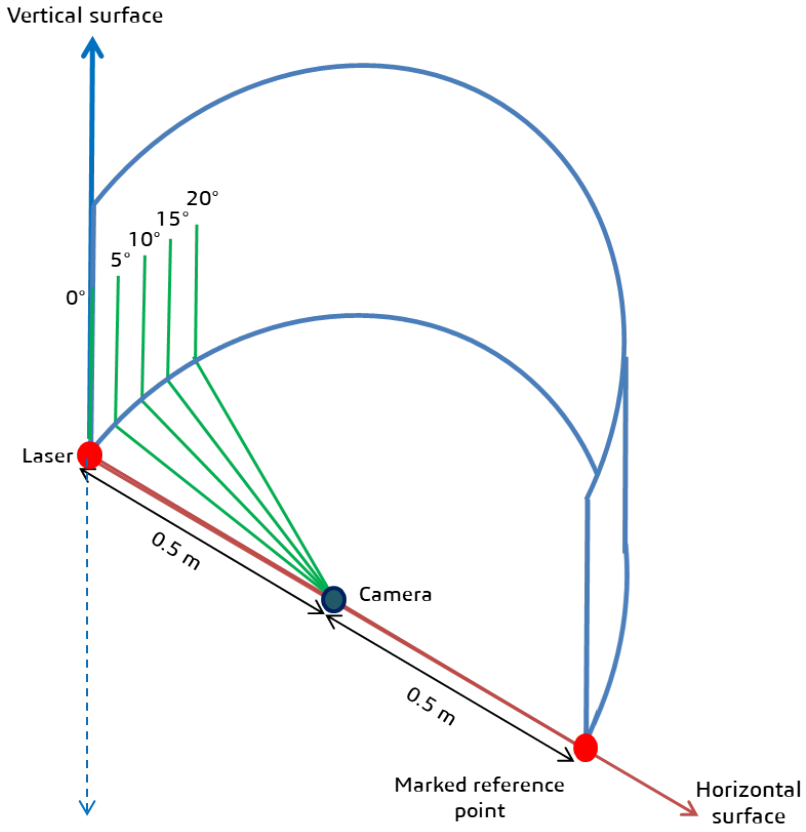

Figure 3.11: Isometric scheme of the set up.

Figure 3.12: Aerial view of the camera set up to determine real angle of view of the lens.

Figure 3.13: Photo to determine real angle of view.

(a) 1:1 100% zoom on the left border. (b) 1:1 100% zoom on the right border.

Figure 3.14: Opposite borders of the image as seen with a 100% zoom.

factor thus corresponds to the ratio between the luminance value at each step and the luminance value of the target when facing the center of the camera [13].

Vignetting curves are universal for the same type of lens and model as found out in [7] and [14]. Then, the vignetting curves obtained by [3] for the sigma 8mm f/3.5 fisheye lens with an aperture of f/11 and f/8 are shown in Figure 3.15 and are used in this work as both correspond to the same lens model.

The curves in Figure 3.15 can be approximated by even-order polynomials. The polynomials for the f/8 and f/11 lens vignetting curves are indicated in equations 3.1 and 3.2, respectively, and will be used in Chapter 4 to calibrate the HDR image. In equations 3.1 and 3.2, r refers to the radial position of the pixel in degrees, where zero degrees correspond to the center of the image, and ninety degrees to the border. Additionally, it is assumed that the vignetting function has radial symmetry. The functions:

$$-0.595r^6 - 0.012r^5 + 0.526r^4 + 0.019r^3 - 0.227r^2 - 0.007r = 1, \tag{3.1}$$

and

$$-0.551r^6 - 0.012r^5 + 0.454r^4 + 0.019r^3 - 0.198r^2 - 0.007r = 1, \tag{3.2}$$

describe the vignetting curves for f/8 and f/11 apertures respectively.

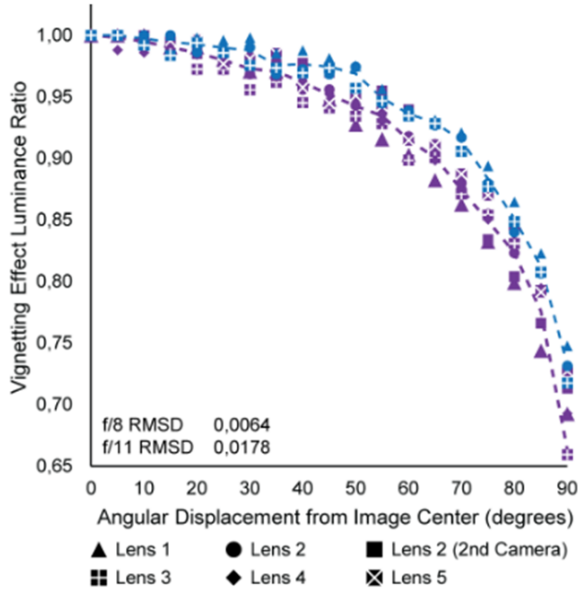

Figure 3.15: Vignetting curves for several Sigma 8mm F3.5 EX DG fisheye lenses where vignetting curves are shown for apertures f/8 and f/11, blue and purple respectively [3].

3.2 Experimental setup

Once the camera lens has been checked for damaged pixels, the setup of the equipment in the scene needs to be done to correctly capture the different exposures of the scene and acquire the luminance and illuminance values that will be used to calibrate the HDR image. The steps to make the complete setup of the equipment used in this thesis for acquiring the set of low dynamic range (LDR) images with different exposure values (also known as bracketing) is explained below. The complete list of the equipment used in this work is presented in Appendix A.

3.2.1 Steps for setup

1. The camera is mounted on a tripod to prevent alignment problems between the acquired LDR pictures.

2. The illuminance meter is attached to the camera and positioned just above the fisheye lens as shown in Figure 3.16. Attention should be paid in the alignment of the border of the illuminance meter with the border of the camera lens.

3. The camera is connected via USB to a computer with a UNIX environment where the software qDslrDashboard to remotely control the camera has been previously installed.

4. The settings of the camera with an f/8 aperture are defined in qDslrDashboard as shown in Figure 3.17.

5. The bracketing settings are defined in qDslrDashboard, where 1 EV separation between the low dynamic range (LDR) images is recommended in [22]. See Figure 3.17.

6. A grey card is positioned somewhere on the scene with mid-range luminance values within the fisheye lens field of view.

7. The luminance meter is positioned near the camera fisheye lens and pointing to the center of the grey card.

During the bracketing process the vertical illuminance value of the scene, as well as a spot luminance measure from the grey card should be taken. These measurements will be further used to calibrate and validate the final high dynamic range (HDR) image from which a luminance map will be derived.

The illuminance meter is used to acquire the vertical illuminance of the scene. As the illuminance can vary during the bracketing process, the illuminance meter is set to measure in average mode, where the illuminance values, from the beginning of the bracketing until the process has finished will be recorded, ant the average illuminance will be output. This is the value that will be used to validate the image. Additionally, during the bracketing process, a spot luminance measurement of the grey card is done with the luminance meter. The luminance meter is placed near the camera and points towards the grey card. The spot luminance value acquired will be used to make the photometric calibration of the HDR image, as explained in the next chapter. The setup diagram of the equipment is shown in Figure 3.18.

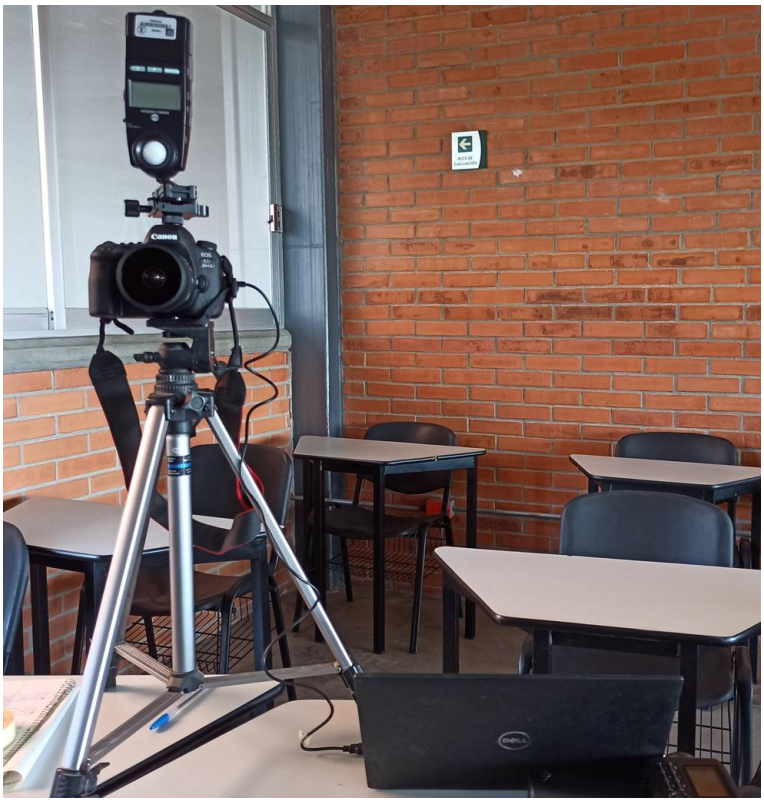

Figure 3.16: Illuminance meter positioned above the fisheye lens.

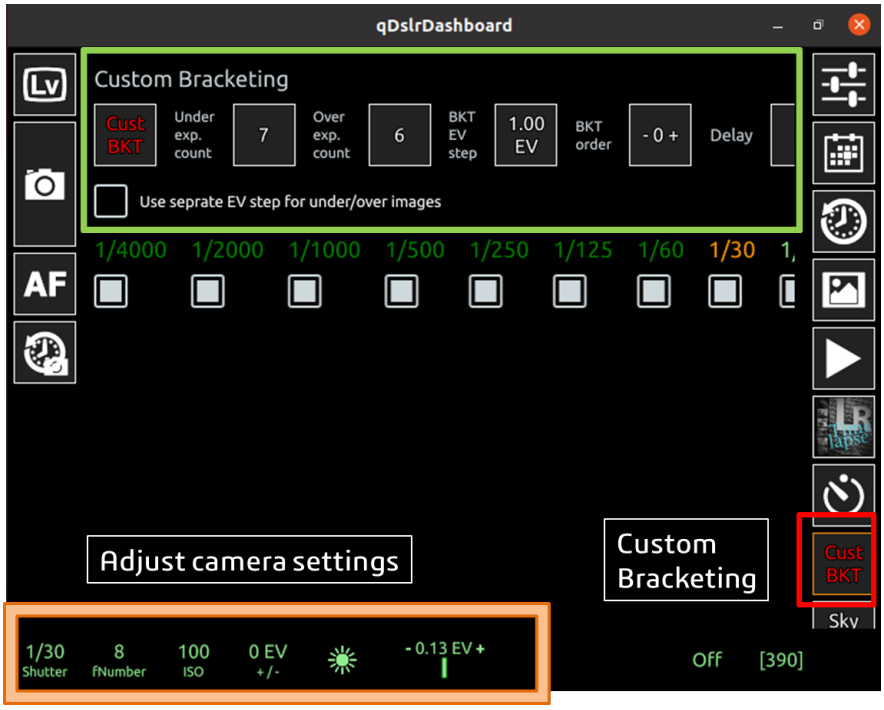

Figure 3.17: Interface in qDslrDashboard to adjust camera settings and bracketing.

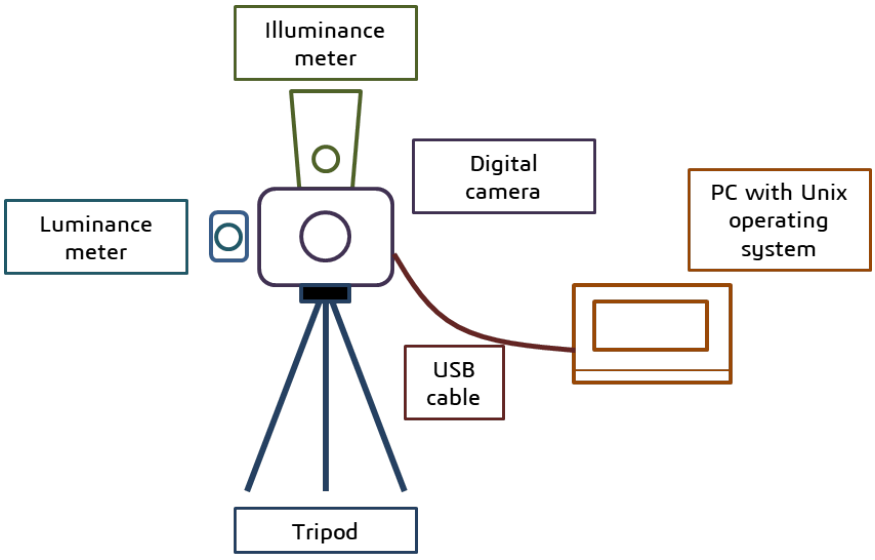

Figure 3.18: Diagram of the hardware to acquire low dynamic range (LDR) pictures.

CHAPTER 4

HDR image generation and calibration

In this chapter the complete process to generate a high dynamic range (HDR) image from a set of low dynamic range (LDR) images with different exposure values is explained, followed by the process to calibrate the HDR image in order to obtain an accurate luminance map from it. First, in section 4.1 the process to capture multiple pictures with different exposure values, also known as bracketing is presented. Next, the selection of exposures is done to cover the complete dynamic range of a scene. Then, the procedure to merge LDR images is described. After the HDR image is created, section 4.2 describes the steps needed to calibrate this image with the process to obtain a luminance map from it. Finally, in section 4.3 the steps to identify the glare sources of a scene from a calibrated HDR image are presented.

4.1 HDR image generation

4.1.1 Capture of different exposures

The process of taking several pictures from underexposed to overexposed is called bracketing. During bracketing, fixed mid aperture lens values (e.g f/11 or f/8) are suggested in [22]. Bigger aperture values would lead to an increment of vignetting [7] while smaller apertures can produce lens flare [14]. Furthermore, camera settings should be fixed according to the recommended literature values [23], shown in Table 4.1.

Setting	Value
Film speed	ISO 100
White balance	Daylight (5200K)
Exposure mode	Manual
Light metering mode	Not important
Focus mode	Manual
Focus value	Infinite
Image quality	Largest (when using JPEG)
Image type	JPEG or RAW
Picture style	Neutral
Peripheral illumination correction	Disabled
Color space	sRGB

Table 4.1: Recommended settings for the camera during the acquisition of LDR images [23].

The capture of the different exposures should be done by varying the exposure time rather than the aperture value of the lens, since changing aperture values would add to the vignetting effect [13]. The ISO value is set to 100 to avoid additional noise in the images. It is recommended to take a set of at least 15 images, to capture the complete dynamic range of the scene. However, the number of images could vary depending on the scene conditions [22] e.g. scenes with a high contrast, like a sunset, will usually require more images to capture their complete dynamic range.

The pictures are taken in RAW format to avoid losing valuable information about the scene illumination, as they contain the unprocessed data from the image sensor, from which the camera response function can be directly derived when merging the pictures.

For the bracketing, qDslrDashboard is used to specify the camera settings (see Chapter 3 section 3.2 according to the recommended values in Table 4.1). The bracketing is configured to capture the images with 1 EV stop difference between them, and a total of 15 images are taken.taken. Exposure times longer than 3 seconds are avoided, as daylighting conditions are likely to vary. A set of LDR images taken with the bracketing process is shown in Figure 4.1. Additionally, during the whole bracketing process the time average illuminance of the scene is recorded with the illuminance meter T-10A placed above the camera lens, and a luminance measurement of the grey card is taken with the luminance meter LS-160 as explained in section 3.2.

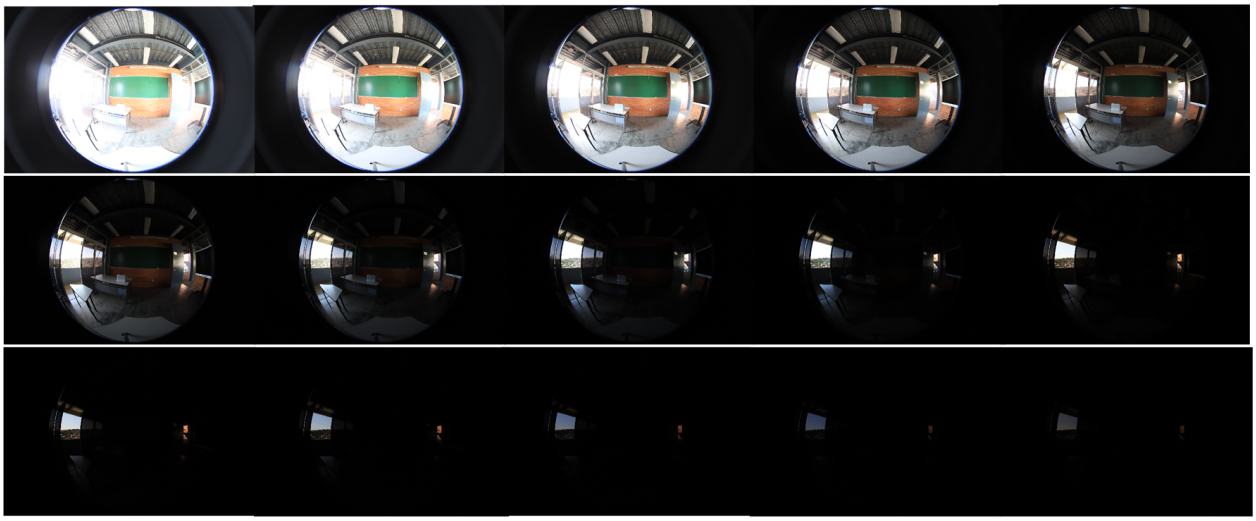

Figure 4.1: Set of 15 images with variable exposure time from 2.5 s to 1/4000 s separated by 1 EV stop.

4.1.2 Exposure selection

The set of LDR images contains the darkest and the brightest exposure, corresponding to the shortest and longest exposure time of the bracketing process respectively. This exposure time is subjectively defined depending on the scene brightness. To ensure that a set of LDR images actually comprises the complete dynamic range of a scene, an exposure selection needs to be done. During this process the darkest and brightest images are reviewed, and for the set to be useful, the former should have no pixels where the R, G and B values are simultaneously over 228, while the latter should not have pixels where they are simultaneously below 27 [22]. Within this interval it is ensured that in the darkest exposure the total luminance in the field of view has been captured by the sequence [22], which is especially important for glare analysis.

In this work, to find out if there are any pixel channel values simultaneously equal or greater than 228 in the darkest exposure or any pixel channel values simultaneously equal or lower than 27 in the brightest one, the according raw images are processed using rawpy and the following Python commands:

```
raw=rawpy.imread("image.CR2")
raw_array=raw.postprocess()
```

A raw color image is represented by a 3D matrix which gives the coordinates of the pixel and its RGB values. In this work, the combination of camera and lens outputs a circular fisheye image, which means that the scene picture is shown in a circle inscribed and centered on the camera sensor. As discussed in section 3.1, the electronics of the sensor can generate noise in the pictures as can be seen in Figure 3.2. To remove the noise caused by the pixels that do not belong to the scene inscribed in the circle of the picture, all pixels outside the circle are masked to black for the underexposed image and to white for the overexposed image. This will ensure that in the further analysis, any black or white pixel found corresponds to a point of the scene in the circle. The pixel-angle relationship obtained in Chapter 3 section 3.1.4 is used to obtain the total amount of pixels within the sensor that comprises the complete angle of view of the lens. In order to set all the pixels outside the fisheye lens to either white or black

values, and having a camera sensor composed of 6264x4180 pixels, a Python script is written, where the coordinates of the center of the fisheye image are defined, as well as the circle radius in pixels. The code then identifies those pixels that do not belong to the circular fisheye and sets their RGB values to either black (i.e [0,0,0]) or white (i.e [255,255,255]). The code to mask the pixels outside the circle to black is shown below. In the code, everytime a pixel that does not belong to the circle is found, its RGB values are set to black. To mask an overexposed image the color value of the pixel should be defined to white i.e. change 0 for 255 in the fifth line of the code.

```
cx=4180/2
cy=6264/2
r=2050
araw=[]
black=np.full((1,1,3), 0, dtype=int)

for i in range(len(raw_array)):
    for j in range(len(raw_array[i])):
        x=i-cx
        y=j-cy
        if((x**2+y**2)<=r**2):
            araw.append(raw_array[i][j])
        else:
            araw.append(black[0][0])

raw_new=np.array(araw)
raw_new=raw_new.reshape(4180,6264,3)
```

Finally, in an underexposed image the number of pixels having RGB values greater than 228 can be found with the following script:

```
count_raw=raw_new.sum(axis=2)
count=count_raw.reshape(4180,6264,1)
raw_true=((count[:,:]>=684))
np.count_nonzero(raw_true)
```

and to find pixels having RGB values lower than 27 in the overexposed image, the script is as follows:

```
count_raw=raw_new.sum(axis=2)
count=count_raw.reshape(4180,6264,1)
raw_true=((count[:,:]<=81))
np.count_nonzero(raw_true)
```

The flowchart that represents the code described above to mask the image and find out if there are any pixels having RGB values greater than 228 for an underexposed image or pixels with RGB values lower than 27 for an overexposed image is shown in Figure 4.2.

If any pixels with RGB values greater that 228 are found in the underexposed image, then the exposure time during the bracketing process should be reduced until no pixel with this values is found on the underexposed image. Also, if any pixels with RGB values lower than 27 are found in the overexposed image, the exposure time during the bracketing process should be increased until no pixel with this values is found on the overexposed image. After the darkest and brightest exposures complying with the previously defined conditions have been selected, the pictures in between them can be merged to create the HDR image.

4.1.3 Merging exposures

Once useful exposures are selected, LDR images are merged to obtain an HDR image which will contain the relative luminance values of every point in the scene. Each pixel in the camera sensor records an intensity value corresponding to a nonlinear function of the original exposure at that pixel. The original exposure refers to the product of irradiance times the exposure time, and the non-linear function that relates the intensity value of a pixel to the scene radiance

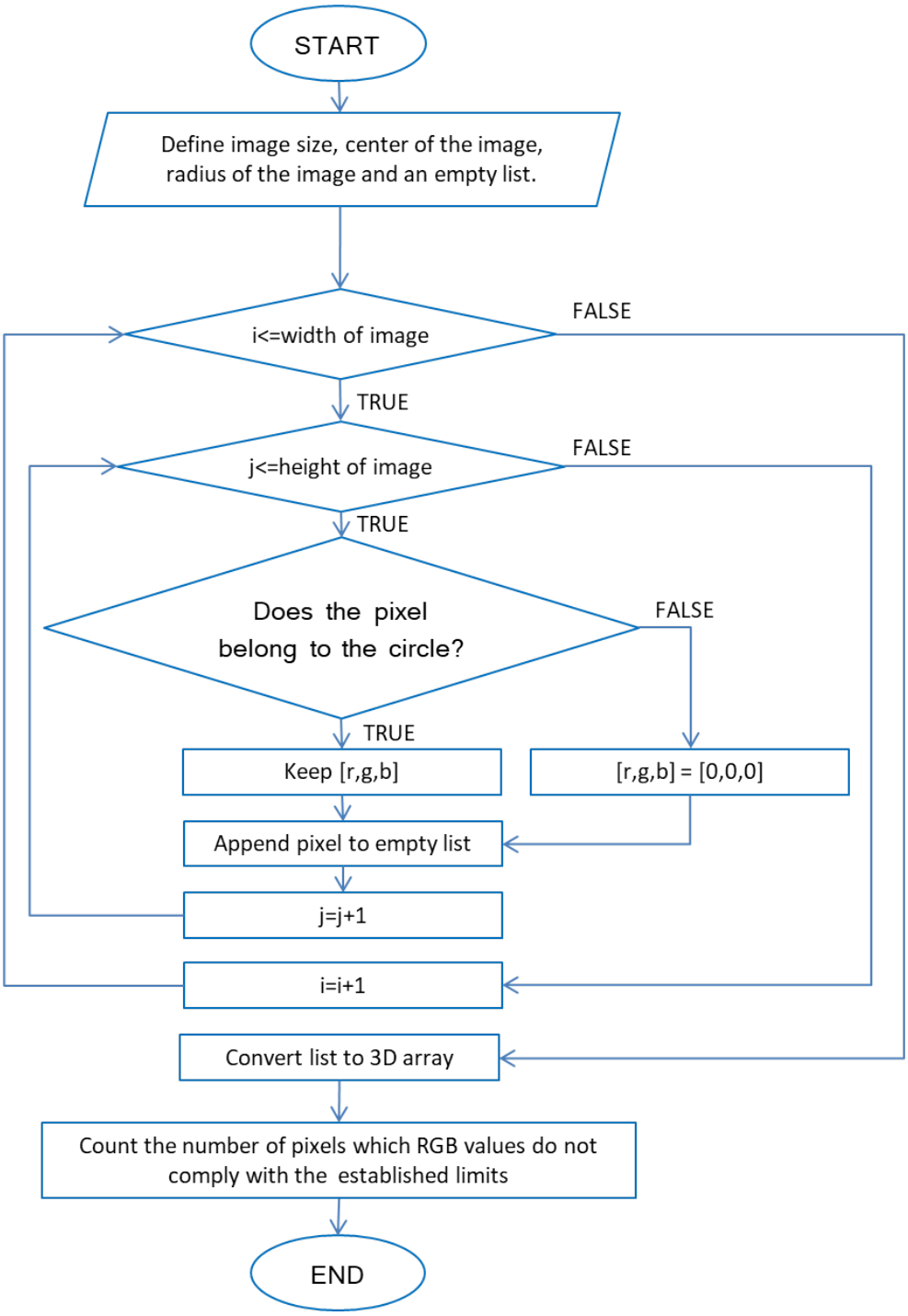

Figure 4.2: Flowchart to mask the image and find out if there are any pixels having RGB values greater than 228 for an underexposed image or pixels with RGB values lower than 27 for an overexposed image.

is the camera's response curve and varies according to the camera model. When pictures are merged to output an HDR image, each pixel among the different pictures has different intensity values, and as LDR images vary from underexposed to overexposed, pixels will have maximum and minimum values along with the entire set. In order to achieve the true relative value of each pixel, a weighting function is defined to give a major influence to the mid pixel values. Then weighted arithmetic mean can be performed for each pixel, acquiring the relative intensity values of every point in the scene [11]. To combine the LDR images and create an HDR image as shown in Figure 4.3, the Radiance tool *raw2hdr* is used typing the following command on the terminal, where the set of RAW images from the bracketing is specified as input by IMG*.CR2:

```
raw2hdr -a -e -f -g -h -w -o image.hdr IMG*.CR2
```

which after combining the LDR images outputs an HDR image that can be visualized with the command ximage as follows:

```
ximage image.hdr
```

Figure 4.3: HDR image created from the set of fifteen LDR images shown in Figure 4.1.

4.2 HDR image calibration

Once an HDR image has been created, the calibration must be done to the HDR image prior to deriving an accurate luminance map from it. The calibration process includes nullifying the exposure value of the HDR image created, cropping and resizing, applying a vignetting correction, making a photometric adjustment, and editing the image header. It should be noted that during this work no neutral-density filters (ND) are used. The ND filters reduce the amount of light that enters a camera lens. If an ND filter is used during the LDR image acquisition an additional calibration step must be made to account for the chromatic shift and brightness scaling produced by the filter [22].

4.2.1 Nullification of exposure value

When creating an HDR image, a header including the settings and parameters of the image is contained and can be visualized with the following command:

```
getinfo image.hdr
```

which will output, as an example:

```
#?RADIANCE
CAMERA= Canon EOS 6D Mark II version dcraw v9.28
hdrgen created HDR image from 'IMG_1.tif' 'IMG_2.tif' 'IMG_3.tif' 'IMG_4.tif'
'IMG_5.tif' 'IMG_6.tif' 'IMG_7.tif' 'IMG_8.tif' 'IMG_9.tif' 'IMG_10.tif'
'IMG_11.tif' 'IMG_12.tif' 'IMG_13.tif' 'IMG_14.tif' 'IMG_15.tif'
Removed lens flare
EXPOSURE=6.201528e-02
CAPDATE= 2020:11:05 01:34:32
PRIMARIES= 0.6400 0.3300 0.3000 0.6000 0.1500 0.0600 0.3127 0.3290
FORMAT=32-bit_rle_rgbe
```

However, after an HDR image is created, the exposure value contained in the header should be directly included in the pixel values to avoid later compilation errors [22]. The Radiance tool *raw2hdr* is used to include the exposure value in the pixels and to remove the wrong exposure value that is automatically included on the header, which avoids further compilation errors. The command for this should be used right after creating the HDR image as follows:

```
ra_xyze -r -o image.hdr > image_nullEV.hdr
```

when the exposure value has been set in the pixels, it will be nullified from the header. To verify this, we use the Radiance command:

```
getinfo image_nullEV.hdr
```

which outputs a header that no longer contains an exposure value:

```
#?RADIANCE
CAMERA= Canon EOS 6D Mark II version dcraw v9.28
hdrgen created HDR image from 'IMG_1.tif' 'IMG_2.tif' 'IMG_3.tif'
'IMG_4.tif' 'IMG_5.tif' 'IMG_6.tif' 'IMG_7.tif' 'IMG_8.tif'
'IMG_9.tif' 'IMG_10.tif' 'IMG_11.tif' 'IMG_12.tif' 'IMG_13.tif'
'IMG_14.tif' 'IMG_15.tif'
Removed lens flare
CAPDATE= 2020:11:05 01:34:32
ra_xyze -r -o image.hdr
PRIMARIES= 0.6400 0.3300 0.2900 0.6000 0.1500 0.0600 0.3333 0.3333
FORMAT=32-bit_rle_rgbe
```

4.2.2 Cropping and resizing

As the image from the scene is contained in a circle inscribed in the rectangular camera sensor, cropping the image into a square containing the fisheye view will ease the following analysis and image visualization. However, cropping the image is not mandatory, and skipping this step does not have an impact on the further calibration steps.

The cropping of the image is made with the Radiance tool *pcompos*, in which the dimensions (in pixels) of the square that will encompass the fisheye view have to be defined and corresponds to the fisheye diameter. The anchor point coordinates from which the image will be cropped has to be defined as well and it is by default positioned on the lower left corner of the image, unless otherwise stated. It should be noted that if the command *-h* has been included in *raw2hdr* when merging the multiple exposures, coordinates of the anchor point should be defined according to the new image dimensions, as using *-h* outputs a half-size image. In addition, when cropping an HDR image, the viewing type and viewing angle contained in the image header are nullified and have to be corrected as a final step during the HDR image calibration.

The command used in this work to crop the HDR for a 26 MP image is:

```
pcompos -x 2060 -y 2060 image_nullEV.hdr -550 -10 > image_crop.hdr
```

Furthermore, in this work luminance maps derived from HDR images are used to detect glare sources within the scene using the Radiance tool *evalglare*. As evalglare requires the image input to be smaller than 1500x1500 pixels it is necessary to resize the image. This can be done using the tool *pfilt*, where the x and y define the output resolution of the image is defined in pixels and the -1 command is indicated to avoid adding an exposure value to the image header [22]. During this work an output image of 1000x1000 pixels is defined as recommended in the *evalglare* documentation. The command to resize the image is written as follows:

```
pfilt -1 -x 1000 -y 1000 image_crop.hdr > image_resize.hdr
```

The dimensions of the output image can be modified if needed, and if it is not required, image size could remain the same. A cropped and resized image is shown in Figure 4.4.

Figure 4.4: HDR image after cropping and resizing.

4.2.3 Vignetting correction

As described in Chapter 2, vignetting effect causes pixel brightness to decrease from the center to the periphery of an image. In order to accurately retrieve the relative luminance values from an image, pixels should be compensated for the vignetting effect. The vignetting curves shown in Figure 3.15 describe the vignetting factor that needs to be applied to each pixel depending on its radial position to compensate for the vignetting effect [22]. The luminance values of the pixel after the vignetting correction in each channel $R_0(r)$, $G_0(r)$, and $B_0(r)$ are retrieved with equations 4.1,4.2, and 4.3 respectively, where $R_i(r)$, $G_i(r)$, and $B_i(r)$ are the original luminance values, as a function of the radius r of the image, without applying a vignetting correction, and $f_v(r)$, the vignetting correction factor, is the inverse of the polynomial vignetting function (equation 4.4).

$$R_0(r) = f_v(r) * R_i(r), \tag{4.1}$$

$$G_0(r) = f_v(r) * G_i(r), \tag{4.2}$$

$$B_0(r) = f_v(r) * B_i(r), \tag{4.3}$$

and

$$f_v(r) = \frac{1}{ar^k + br^{k-1} + ... + nr + 1}. \tag{4.4}$$

To apply the corresponding vignetting factor to each pixel in the cropped and resized HDR image, a plain text file having a .cal extension is created. In it, the diameter of the fisheye view (in pixels) is defined, along with its center coordinates and equations 4.1, 4.2, 4.3, and 4.4. The code to define the vignetting functions is shown below, and k should be substituted according to the polynomial order of the vignetting function corresponding to the lens used. For the SIGMA fisheye lens used during this thesis, k=6 as shown in equations 3.1 and 3.2.

```
xr=(x-imagesize_x/2);
yr=(y-imagesize_y/2);
sq(xr)=xr*xr;
sq(yr)=yr*yr;
r=(sqrt(sq(xr)+sq(yr)))/image_radius;
Ro=(Ri(1)*(1/((ar^6+br^5+cr^4+dr^3+er^2+fr+1))));
Ro=(Ri(1)*(1/((ar^6+br^5+cr^4+dr^3+er^2+fr+1))));
Ro=(Bi(1)*(1/((ar^6+br^5+cr^4+dr^3+er^2+fr+1))));
```

The coefficients for the polynomial vignetting function are those from equations 3.1 and 3.2 and should be substituted according to the aperture used during the capturing of the LDR images with different exposures. Finally, to apply the vignetting correction to each pixel of the cropped HDR image, the vignetting_file.cal is called within the *pcomb* command as follows:

```
pcomb -f vignetting_file.cal image_resize.hdr > image_vignetting.hdr
```

which will output an HDR image with relative luminance values, and vignetting corrected.

4.2.4 Photometric adjustment by spot luminance

While capturing the set of LDR images, the spot luminance value from a grey card placed somewhere in the scene with mid-range luminance values (as in Figure 4.5) is measured. The ratio (L_r) between the luminance value of the grey card measured with the luminance meter (L_m) and the relative luminance value derived from the HDR image (L_d) corresponds to the scaling factor [22] and is calculated as:

$$L_r = \frac{L_m}{L_d} \tag{4.5}$$

However, as the exact position of the measured luminance value is unknown, instead of deriving a luminance value from a single point in the grey card, an average is made over a selected area of the grey card in the HDR image, and compared to the measured luminance value. In order to calculate the average of the luminance values on the grey card, the grey card is cropped from the image by defining the size in pixels of the crop and the origin as in the following code:

```
pcompos -x $sizex -y $sizey image_nullEV.hdr -$x1 -$y1 >image_crop.hdr
```

Next, the RGB values of each pixel in the crop are retrieved and output to a csv file with the following code:

```
pvalue -h -H -d image_crop.hdr > grey.csv
```

The luminance value of a pixel is calculated in Radiance, knowing the RGB values as shown in [22], with the following expression :

$$L = 179 * (R * 0.2651 + G * 0.6701 + B * 0.0648) \tag{4.6}$$

where L is the luminance of the pixel in $[\frac{cd}{m^2}]$, 179 is the standard luminous efficacy in Radiance $[\frac{lm}{W}]$, R, G, and B are the spectrally weighted radiance of the pixel $[\frac{W}{m^2 \cdot sr}]$, and the parameters 0.2651, 0.6701, 0.0648 are calculated from CIE chromaticities for the Radiance primaries [22].

Equation 4.6 is introduced in a Python code to calculate the luminance values for each pixel, which are used to calculate the average luminance value of the selected zone of the grey card. Additionally, the standard deviation of the luminance values along the selected zone of the grey card is calculated, to check for the uniformity of luminance over the grey card. The code is as follows:

```
import numpy as np
import pandas as pd

data = pd.read_csv('grey.csv')
data.columns = ['a']
split_data = data["a"].str.split("      ")
dat = split_data.to_list()
names = ["x", "r", "g", "b"]
new_df = pd.DataFrame(dat,columns=names)
del new_df['x']
card = new_df.to_numpy()
lum=[]

for i in card:
    r=float(i[0])
    g=float(i[1])
    b=float(i[2])
    L=179*(0.2651*float(r)+0.6701*g+0.0648*b)
    lum.append(L)

print(np.mean(lum))
print(np.std(lum))
```

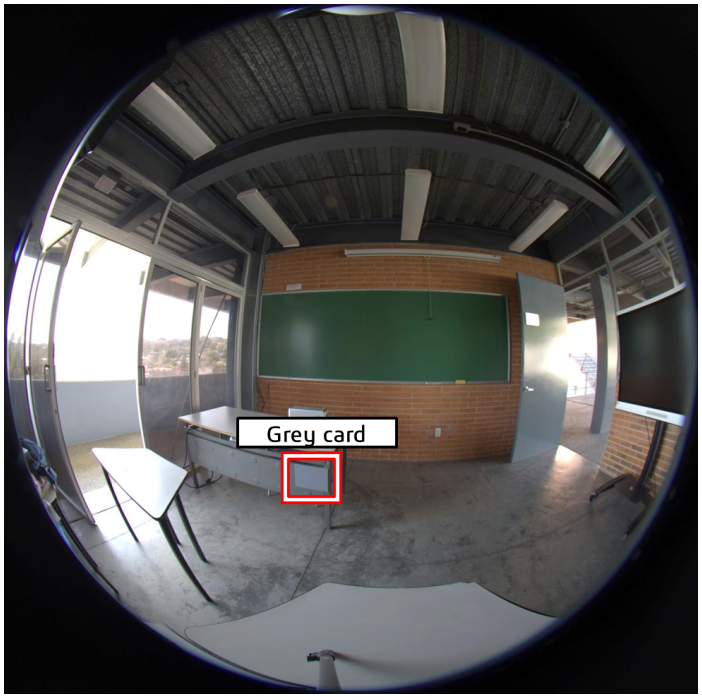

Figure 4.5: Example of positioning of a grey card in the scene.

The flowchart that describes the code above explained to calculate the average luminance value of the selected zone of the grey card is shown in Figure 4.6.

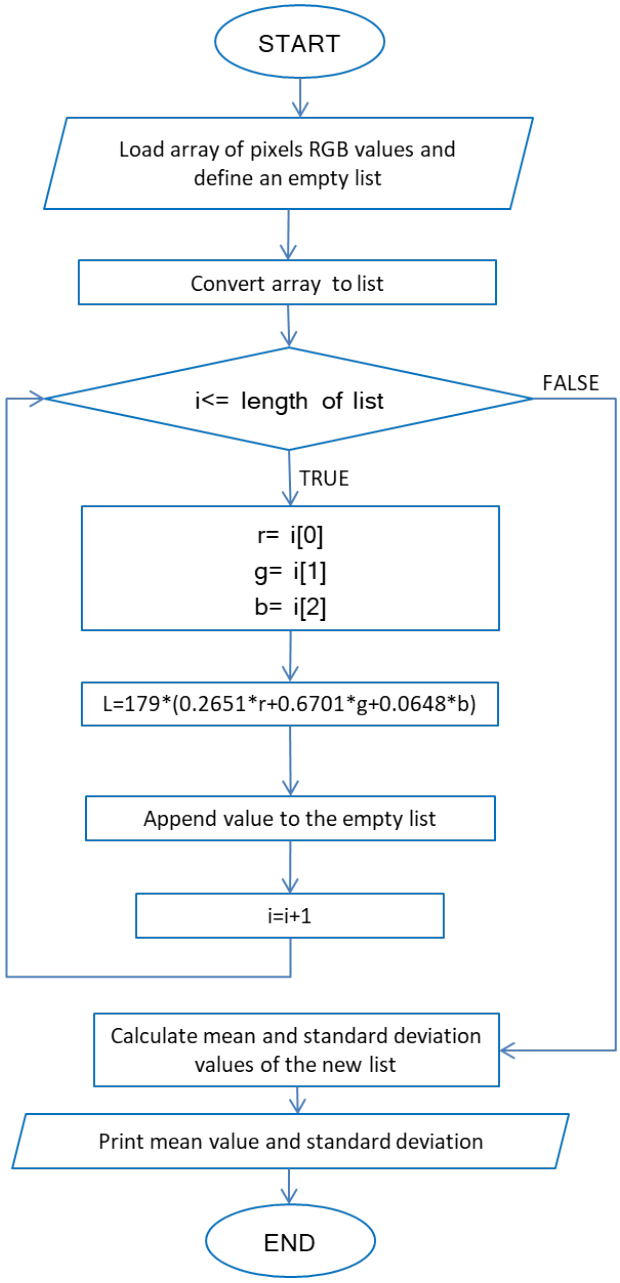

Figure 4.6: Flowchart to obtain the average luminance value of the selected zone of the grey card.

As stated before, combining a set of LDR images will create an HDR image that contains the relative luminance values of a scene. In order to obtain the real luminance values of the scene, each pixel from the image needs to be multiplied by the scaling factor of equation 4.6. The luminance values of the pixels from the image are multiplied by the scaling factor using the *pcomb* tool in a command as follows:

```
pcomb -s factor image_vignetting.hdr > image_photometric.hdr
```

4.2.5 Header editing

The last step before deriving a luminance map from a calibrated HDR image is editing the header. This needs to be done before doing any image post-analyses as the results for glare are usually dependant on the solid-angle of each pixel and angular relations within the image [22]. Therefore, the image header should contain the lens projection type and the real angle of view. These parameters can be defined using the getinfo command, where equidistant and orthographic projections for the fisheye lens are defined with -vta and -vth respectively, and the real viewing angle of the lens in both vertical and horizontal axis should be entered in degrees, for -vv and -vh.

For this work, as mentioned before, the lens has an equidistant projection and the real angle of view was found to be 186°. Then, the code line to add this information to the image header is as follows:

```
getinfo -a "VIEW=-vta -vv 186 -vh 186" < image_photometric.hdr > image_header.hdr
```

4.2.6 HDR image validation

Once an HDR image has been generated and calibrated, a validation needs to be done to ensure the HDR image represents the accurate luminance values from the scene. The validation of the HDR image is done by comparing the measured illuminance value of the scene (E_m), which is retrieved during the bracketing process with the illuminance meter, with the illuminance value of the scene derived from the image (E_d).

Before deriving the illuminance value of the scene, a mask should be applied to the HDR image for it to represent a 180^o angle of view. This will allow comparing the derived luminance value of the HDR image with the measured illuminance value, as the illuminance meter has a 180 ^{o} angle of view. To mask the HDR image, the Radiance tool *pcomb* is used. In the command line, the center of the HDR image is defined, along with the radius in pixels that corresponds to a 180^o field of view. Then, a function is defined where all the pixels not belonging to the 180^o field of view in the HDR image are set to black (i.e.[0,0,0]). The command to do this is as follows, where the HDR image with a 180^o field of view (image_final.hdr) will be the output:

```
pcomb -e 'Cx:xmax/2; Cy_ymax/2; R:500; sq(x):x*x'
-e 'inC=sq(R)-sq(x-Cx)-sq(y-Cy)'
-e 'ro=if(inC,ri(1),0);go=if(inC,gi(1),0);bo=if(inC,bi(1),0)'
-o image_header.hdr > image_final.hdr
```

Once the pixels outside the 180° field of view have been masked to black, the illuminance value from the HDR image can be derived using the *evalglare* command as follows:

```
evalglare -V image_final.hdr
```

which will output the vertical illuminance value of the scene.

Then, both measured and derived illuminance values of the scene can be compared to calculate the percent error of the image with equation 4.7,

$$e = \frac{E_d - E_m}{E_m} 100. \tag{4.7}$$

According to [22], if the error between measured and derived illuminance values is higher than 25% , the image should be discarded, and usually an error below 10% should be expected.

4.2.7 Generation of luminance maps

Once the HDR image is calibrated and validated, its luminance map is derived with the *falsecolor* tool, where the maximum luminance value of the scale, as well as the logarithmic mapping, are defined according to the desired analyses. In this work, the maximum luminance value is set to 5000 $\frac{cd}{m^2}$ and a logarithmic scale is used as follows:

```
falsecolor -s 5000 -i image_final.hdr -e -log 3 > image_luminance_map.hdr
```

4.3 Luminance and glare evaluations

The generated luminance maps can be used to acquire information from the scene, such as detecting glare sources, calculating the daylight glare probability value (DGP), the number, size and position of glare sources in a scene, and retrieving luminance values from the entire scene or zones using the tool *evalglare*.

4.3.1 Glare

To identify the glare sources in a scene, the tool evalglare is used, which has three implemented methods to evaluate glare sources: the factor method, the threshold method, and the task area method. Evalglare identifies glare sources depending on the method used, and calculates the daylight glare probability (DGP). When a check file -c is specified, the output shows the image of the scene with the detected glare sources colored while the rest of the image is set to grey. It should be noted that the color assigned to the glare sources is randomly chosen, and has no meaning. Additionally, using the option -d will print the number of glare sources found within the scene, along with their position, size in pixels, and the maximum and minimum luminance values in the scene.

In this work, glare sources are identified using the threshold method as suggested in [21], due to the high illuminance values. To calculate the DGP and identify glare sources from a luminance map, using the threshold method, the 2000 $\frac{cd}{m^2}$ threshold is preferred as suggested by [21] and is defined in the following command:

```
evalglare -c glare_sources.hdr -b 2000 -d image_luminance_map.hdr > glare_info.txt
```

this will output an hdr image file "glare_sources.hdr" where the identified glare sources are colored while the rest of the image is set to a grey scale. Additionally the DGP values, and the position and size of the identified glare sources will be stored in the file "glare_info.txt".

4.3.2 Specific area analysis

It is also possible to analyze an specific area of a scene by including the -A option with evalglare. To do this, a masking file should be generated, where the center coordinates (x,y) and radius (R) of the desired area are defined, and all pixels outside this area are set to zero. To create a mask from the HDR calibrated image, the command is defined as:

```
pcomb -e 'Cx:x center coordinate; Cy:y center coordinate;
R:area_radius; sq(x):x*x' -e 'inC=sq(R)-sq(x-Cx)-sq(y-Cy)'
-e 'ro=if(inC,ri(1),0);go=if(inC,gi(1),0);bo=if(inC,bi(1),0)'
-o image_final.hdr > mask_file.hdr
```

The output is the mask_file.hdr, an HDR image where all the pixels, except for those corresponding to the specified area to be analyzed, are set to zero value; i.e, black. Then, to obtain the average luminance values of the specified area, along with the maximum luminance values and their standard deviation, the mask file should be included in the command as follows:

```
evalglare -A mask_file.hdr -c glare_sources.hdr -b 2000
-d image_luminance_map.hdr > glare_info.txt
```

This will output on the first lines of the file the average, maximum, and minimum luminance values of the specific zone, along with its standard deviation. Furthermore, the subsequent lines will contain the information regarding the glare sources of the entire original scene and its DGP value.

CHAPTER 5

Experimental results

In this chapter, two experimental campaigns are conducted at IER-UNAM to derive luminance maps are described. In section 5.1, the luminance maps derived from the experimental campaigns are shown, along with the results and the hypotheses of possible sources of error. Then, in section 5.2 the parameters found to show a greater correlation with the error are discussed and presented. Finally, in section 5.3, a glare analysis for different scenes is done, along with the calculation of the daylight glare probability (DGP) of the scenes and a luminance analysis of a specific zone.

5.1 Experimental luminance maps

For this work, two experimental campaigns are conducted at the IER-UNAM. During these campaigns, three different classrooms are selected, and a door aperture is varied for two of them to create different scenes (selecting three different classrooms was preferred over selecting just one classroom under different illumination conditions, as this would have meant a longer experimental campaign, which represented an unnecessary risk under the context of the Covid-19 pandemic). Figure 5.1, Figure 5.2 and Figure 5.3 show the floor plan of classroom 1, classroom 2 and classroom 3 respectively, where the camera position during the experimental campaign is indicated with a red circle. Additionally, Table 5.1 indicates the corresponding classroom for the different scenes, along with the classroom doors that are closed or open for that scene.

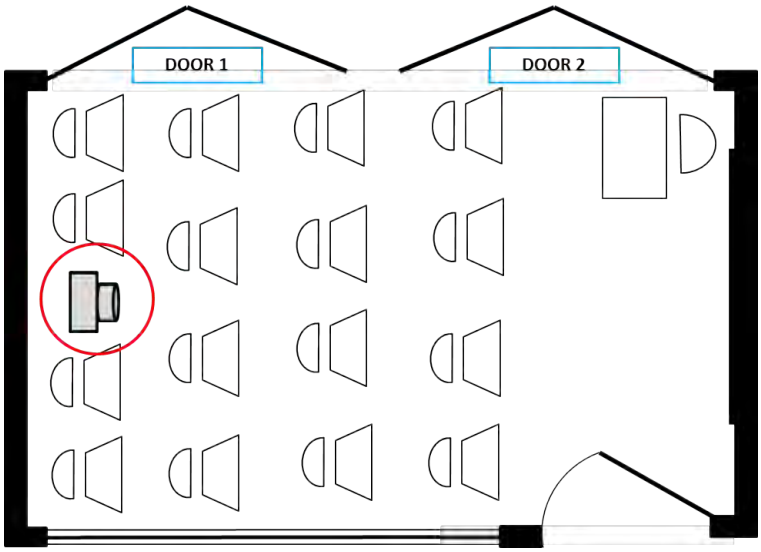

Figure 5.1: Floor plan of classroom 1.

For each scene, luminance maps are derived following the steps of Chapter 3 and Chapter 4. For the first campaign, the grey card is arbitrarily placed somewhere in the scenes, and a luminance map is derived for six different scenes. The luminance maps of the first campaign are shown in Figure 5.4. Then, a second campaign is conducted in the classrooms corresponding to Scenes 3 and 6 of the first campaign; i.e, second and third classrooms.

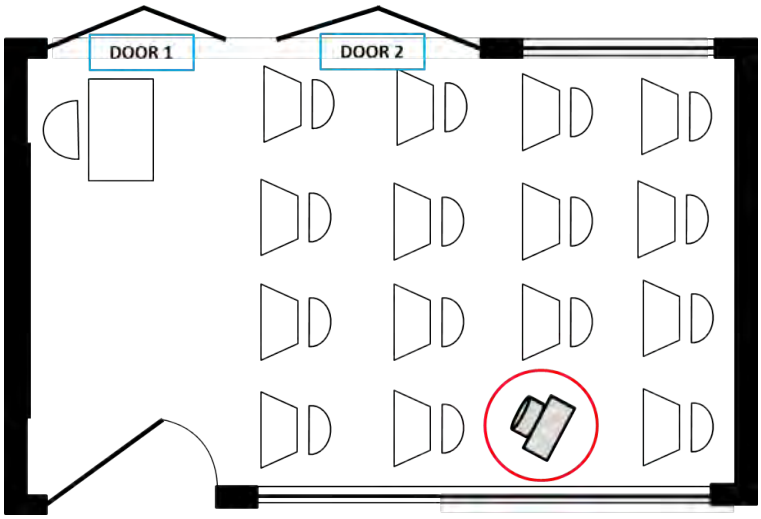

Figure 5.2: Floor plan of classroom 2.

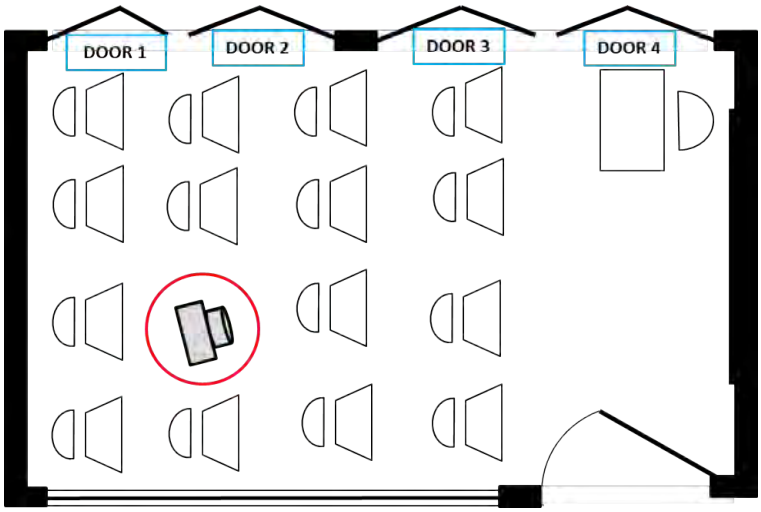

Figure 5.3: Floor plan of classroom 3.

During this campaign, the grey card is placed at six different positions in the scene, as shown in the scheme of Figure 5.5. For each different position of the grey card, a luminance map is acquired, which means a total of twelve luminance maps are generated during the second campaign; i.e, six for each scene. The luminance maps corresponding to Scene 3 are shown in Figure 5.6, and the ones corresponding to Scene 6 are shown in Figure 5.7.

For the first campaign, Figure 5.4 (a) Scene 1 shows the first classroom, in which the lowest luminance values of 5 $\frac{cd}{m^2}$, indicated by the purple color, corresponds to the ceiling of the classroom, while the highest luminance values above 5000 $\frac{cd}{m^2}$, corresponds to the sky, seen through the open door. Figure 5.4 (b) Scene 2 shows the luminance map for the second classroom, in which a door is completely open. Here, the lowest luminance values of 5 $\frac{cd}{m^2}$, correspond mostly to the ceiling, and the highest luminance values above 5000 $\frac{cd}{m^2}$, correspond to the sky seen through the door. In this scene the blackboard is colored with light blue, which according to the scale, corresponds to low mid-range luminance values between 20 $\frac{cd}{m^2}$ and 50 $\frac{cd}{m^2}$. Figure 5.4 (c) Scene 3 shows the luminance map also for the second classroom, but with the door half closed. This clearly has an impact on the luminance of the blackboard, as the map now shows luminance values between 10 $\frac{cd}{m^2}$ and 20 $\frac{cd}{m^2}$, indicated by darker blue color in the border of the blackboard. Additionally, the extent of the low luminance values in the ceiling is increased. Figure 5.4 (d) Scene 4 shows another luminance map for the second classroom; however, for this scene the door of the classroom is completely closed. This drastically decreases the luminance values inside the classroom, by 20 $\frac{cd}{m^2}$ to 40

Scene	Classroom	Door 1	Door 2	Door 3	Door 4
1	1	open	closed	n/a	n/a
2	2	open	open	n/a	n/a
3	2	closed	open	n/a	n/a
4	2	closed	closed	n/a	n/a
5	3	closed	open	closed	closed
6	3	closed	closed	closed	closed

Table 5.1: Classroom configuration for the different scenes.

$\frac{cd}{m^2}$, as most of the scene is now represented by purple and dark blue colors, except for the door, which is colored in orange. Then, Figure 5.4 (e) Scene 5 shows the luminance map of the third classroom. In this scene one of the doors is opened, and most of the scene is represented by a light blue color, which indicates low mid-range luminance values, between 20 $\frac{cd}{m^2}$ and 50 $\frac{cd}{m^2}$. Finally, Figure 5.4 (f) Scene 6, shows a luminance map for the third classroom with all its doors closed. This decreases the luminance values corresponding to the blackboard and the left part of the scene by 20 $\frac{cd}{m^2}$ to 30 $\frac{cd}{m^2}$, which are now represented with dark blue and purple colors.

For the second campaign, Figure 5.6 shows the luminance maps acquired for the classroom of Scene 3. Here, the door of the classroom is completely open. The lowest luminance value of 5 $\frac{cd}{m^2}$ corresponds to the ceiling of the classroom, colored with purple, while the highest luminance values, above 5000 $\frac{cd}{m^2}$, correspond to the sky seen through the door and colored with yellow. Most of the remaining parts of the scene have a light blue color, which indicates low mid-range luminance values between 20 $\frac{cd}{m^2}$ and 50 $\frac{cd}{m^2}$. In Figure 5.6 (a) P1, the grey card is placed in the quadrant of position 1 as shown in Figure 5.5. Here, the grey card's luminance value is between 20 $\frac{cd}{m^2}$ and 50 $\frac{cd}{m^2}$ and is colored in light blue. Then, in Figure 5.6 (b) P2 the grey card is placed in position 2, where its luminance value is lower than in position 1, having 5 $\frac{cd}{m^2}$ represented with a purple color. Figure 5.6 (c) P3 shows position 3 of the grey card, where it is also observed to have low luminance values around 10 $\frac{cd}{m^2}$, as it is colored in dark purple. Figure 5.6 (d) P4 shows the grey card in position 4. Here, the grey card is set far away from the camera making, it hard to identify in the luminance map. In this position the grey card is colored in light blue indicating luminance values between 20 $\frac{cd}{m^2}$ and 50 $\frac{cd}{m^2}$. Next, Figure 5.6 (e) P5 shows the grey card set in position 5, facing the camera and with purple color representing its low luminance values around 5 $\frac{cd}{m^2}$. Finally, Figure 5.6 (d) P6 shows the grey card in position 6, a bit further away than in position 5, but still having low luminance values around 10 $\frac{cd}{m^2}$ as it is colored with dark purple.

Next, Figure 5.7 shows the luminance maps acquired for the classroom of Scene 6. In Figure 5.7 (a) P1, the grey card is placed in position 1 and the map is mostly represented by light green and orange colors, indicating high mid-range luminance values between 100 $\frac{cd}{m^2}$ and 1000 $\frac{cd}{m^2}$. From the six luminance maps derived for this scene, this map shows higher luminance values, and a difference is appreciated from the ones shown in the remaining luminance maps. Figure 5.7 (b) P2, shows the grey card placed in position 2, and having low luminance values around 10 $\frac{cd}{m^2}$, as it is colored in dark purple. In Figure 5.7 (c) P3 the grey card is placed in position 3 and far away from the camera, near the blackboard. Here, the card is colored in dark blue, indicating luminance values between 10 $\frac{cd}{m^2}$ and 20 $\frac{cd}{m^2}$. Figure 5.7 (d) P4 shows the grey card in position 4 and colored in light blue, meaning it has low mid-range luminance values between 20 $\frac{cd}{m^2}$ and 50 $\frac{cd}{m^2}$. In Figure 5.7 (e) P5 the grey card is placed in position 5 and has low mid-range luminance values between 20 $\frac{cd}{m^2}$ and 50 $\frac{cd}{m^2}$, as it is colored in light blue. Finally, Figure 5.7 (f) P6, shows the grey card in position 6, completely facing the camera and having low luminance values around 10 $\frac{cd}{m^2}$, represented with dark purple colors.

After the first experimental campaign, the hypothesis is made that the position of the grey card in the scene could have an impact on the accuracy of the luminance maps. That is why different positions for the grey card within the scene, as shown in Figure 5.5, are proposed for the second campaign. Additionally, a second hypothesis is made that the luminance values along the grey card should be uniform. If the luminance values along the grey card are not uniform, then, the derived average luminance value of the grey card L_d could introduce an error when calculating the luminance ratio L_r from equation 4.5, which would make an impact on the photometrical calibration of the image. The uniformity of the luminance values along with the grey card ($\sigma(L_d)$) is obtained by calculating the absolute percentage standard deviation with respect to L_d. After reviewing the luminance maps from the second

campaign, additional parameters that could be related to the error are proposed to be analyzed. The first parameter is the percent luminance value of the grey card with respect to the average luminance value of the scene (P_{card}), which is defined as,

$$P_{card} = \frac{L_d}{L_{sc}} 100, \tag{5.1}$$

where L_d is the average derived luminance of the grey card, and L_{sc} is the average luminance of the scene. Another parameter that is believed to influence the error is the distance between the grey card position in the scene and the camera (d). Also, the dynamic range of the scene (σ (L_{sc})), which is obtained by calculating the standard deviation of the luminance values.

The previously defined parameters are calculated for the different scenes of both the first and second second campaign, and shown in Table 5.2. In this table, the campaign in which the luminance map is obtained (C) is specified, along with the scene (Sc), the grey card position in the scene (P), and the error of the luminance map (e) defined as,

$$e = \frac{E_d - E_m}{E_m} 100, \tag{5.2}$$

where E_m is the measured illuminance value, and E_d is the derived illuminance value.

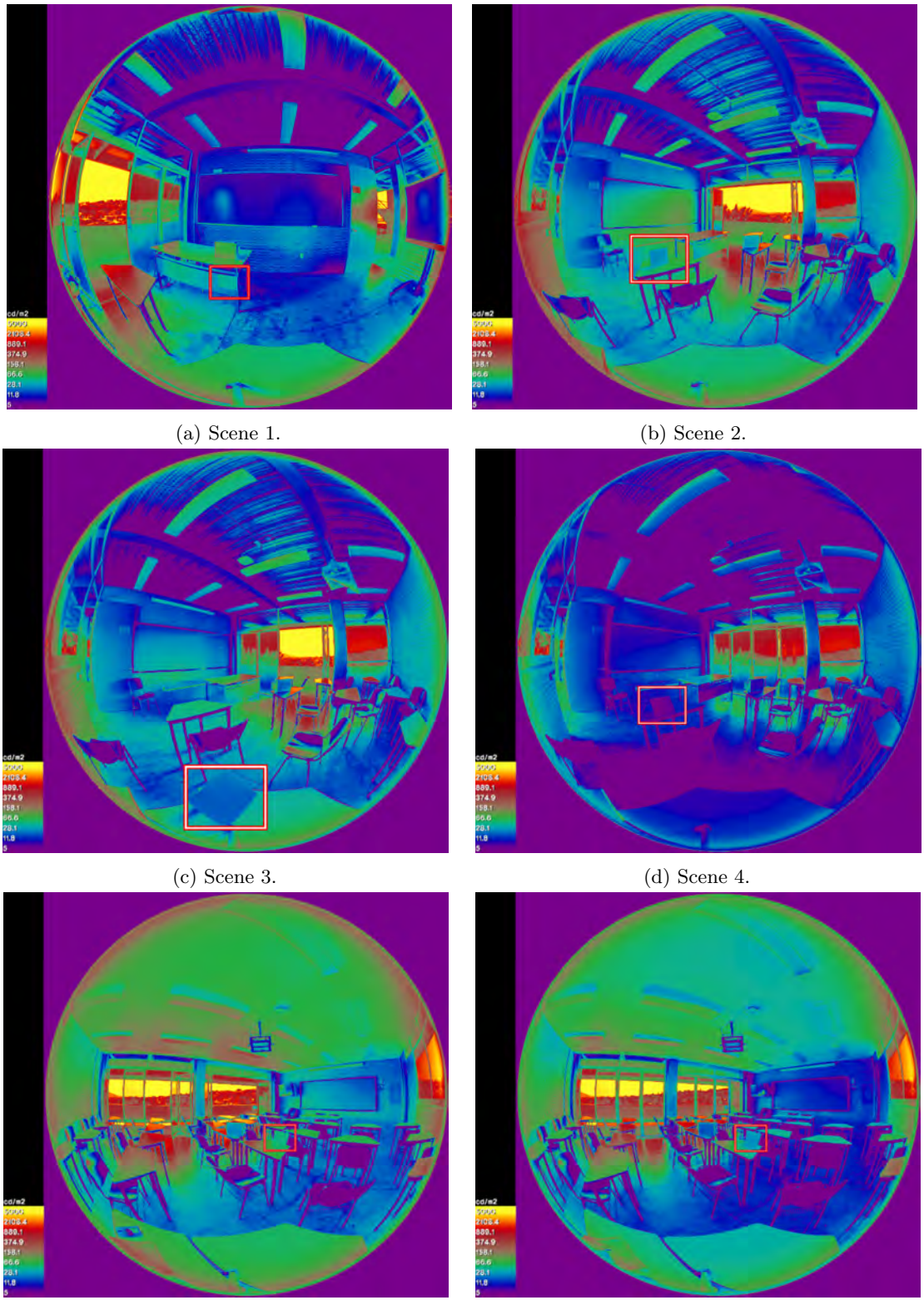

(a) Scene 1.

(b) Scene 2.

(c) Scene 3.

(d) Scene 4.

(e) Scene 5.

(f) Scene 6.

Figure 5.4: Luminance maps of the first campaign derived from HDR images corresponding to six different scenes. The red square outlines the position of the grey card on the scene.

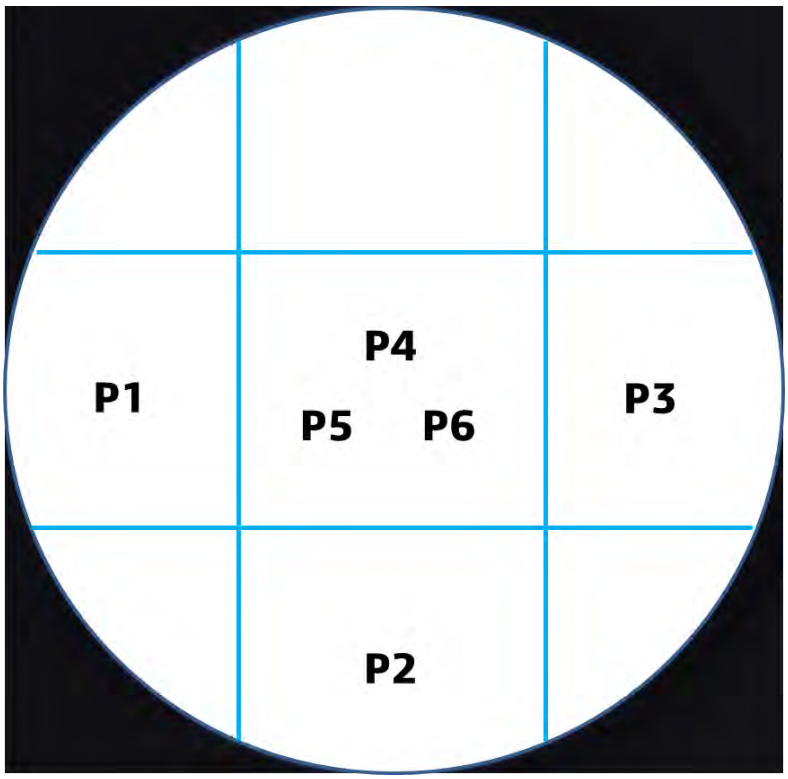

Figure 5.5: Scheme showing the different places the grey card is positioned within the camera lens field of view for the second experimental campaign.

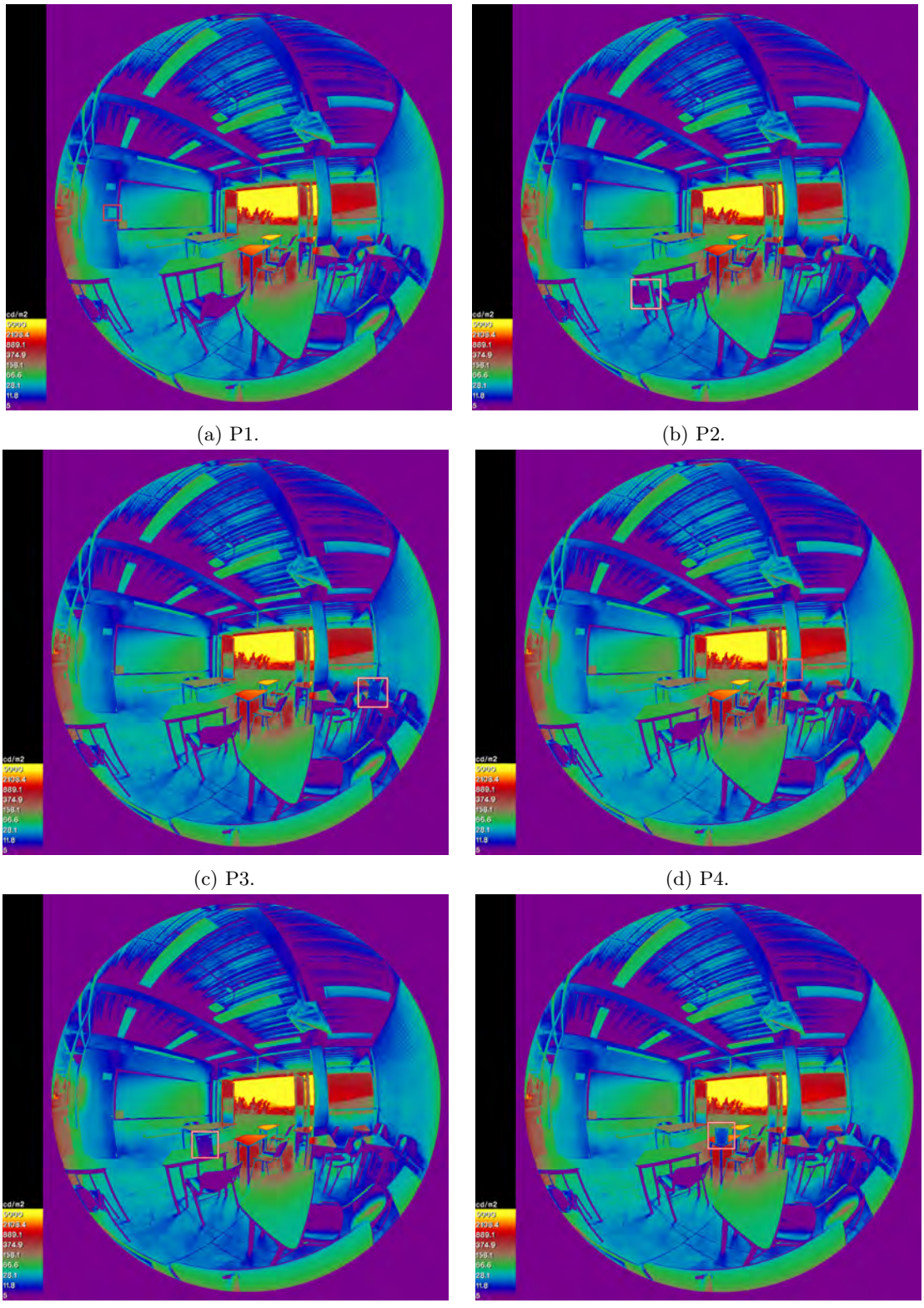

(a) P1. (b) P2.

(c) P3. (d) P4.

(e) P5. (f) P6.

Figure 5.6: Luminance maps of the second campaign for Scene 3 varying the position of the grey card. The red square outlines the position of the grey card on the scene.

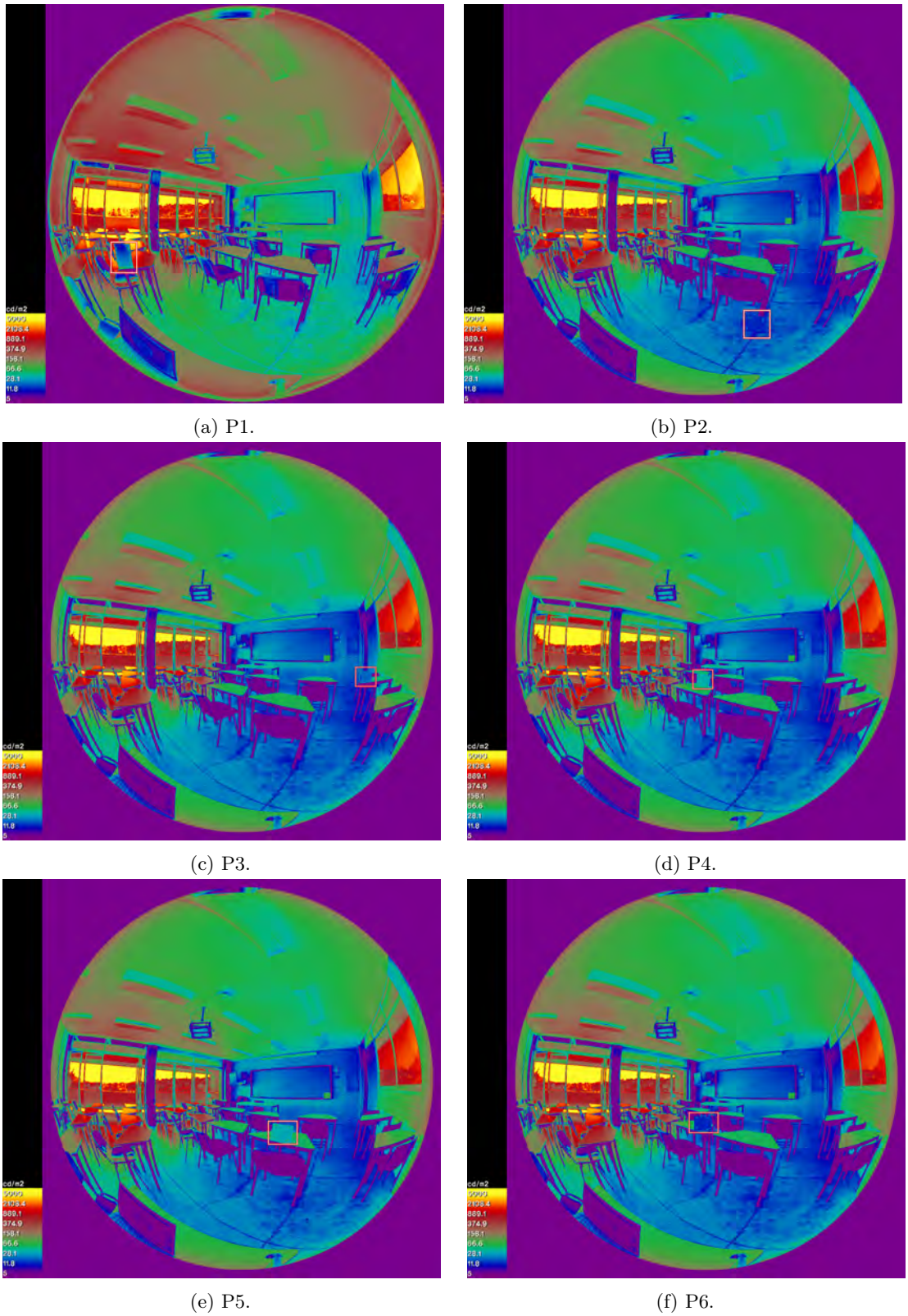

(a) P1. (b) P2.

(c) P3. (d) P4.

(e) P5. (f) P6.

Figure 5.7: Luminance maps of the second campaign for Scene 6 varying the position of the grey card. The red square outlines the position of the grey card on the scene.

C [-]	Sc [-]	P [-]	L_m $[\frac{cd}{m2}]$	L_d $[\frac{cd}{m2}]$	$\sigma(L_d)$ [%]	L_{sc} $[\frac{cd}{m2}]$	P_{card} [%]	d [m]	$\sigma(L_{sc})$ $[\frac{cd}{m2}]$	$L_r[-]$	$E_m[lx]$	$E_d[lx]$	e [%]
1	1	-	36.90	20.70	3.09	242.22	8.55	2.00	1484.20	1.78	427.00	543.60	27
1	2	-	27.40	14.03	6.84	282.21	4.97	1.50	1471.55	1.95	1217.00	1717.00	41
1	3	-	20.20	9.60	2.29	225.06	4.27	0.50	1369.33	2.10	867.00	1632.70	88
1	4	-	6.10	2.80	6.79	42.18	6.64	1.50	178.05	2.18	134.80	212.70	58
1	5	-	46.00	28.60	1.61	232.30	12.31	2.00	1069.65	1.61	889.00	1030.80	16
1	6	-	25.30	14.70	2.93	152.76	9.62	2.00	690.14	1.72	544.00	623.70	15
2	3	P1	28.80	14.30	3.99	300.17	4.76	3.00	1708.92	2.01	1225.00	1707.40	39
2	3	P2	4.90	2.60	6.92	257.20	1.01	1.50	1454.57	1.88	1214.00	1459.00	20
2	3	P3	11.00	5.70	4.04	278.04	2.05	3.00	1577.89	1.93	1200.00	1577.50	31
2	3	P4	19.00	8.30	9.52	322.87	2.57	4.00	1816.99	2.29	1153.00	1825.60	58
2	3	P5	6.50	3.60	4.44	256.37	1.40	2.00	1448.95	1.81	1173.00	1451.70	24
2	3	P6	13.60	6.30	9.52	296.82	2.12	2.50	1690.77	2.16	1211.00	1680.00	39
2	6	P1	15.00	3.00	49.67	571.82	0.52	2.00	3168.60	5.00	611.80	1243.70	103
2	6	P2	11.00	5.20	3.65	238.74	2.18	1.50	1326.34	2.12	617.20	746.50	21
2	6	P3	16.00	7.60	3.68	238.41	3.19	3.00	1322.91	2.11	610.00	746.30	22
2	6	P4	30.40	16.00	5.13	228.43	7.00	2.00	1257.33	1.90	644.00	718.70	12
2	6	P5	30.50	14.40	4.51	235.77	6.11	2.00	1302.93	2.12	636.60	738.80	16
2	6	P6	11.50	5.80	2.07	228.66	2.54	1.50	1260.62	1.98	640.10	717.90	12

Table 5.2: Measured and derived luminance and illuminance values, and the value of different parameters proposed to be analyzed for the luminance maps of the two experimental campaigns conducted at the IER-UNAM, where C is the number of campaign, Sc is the scene, P is the position of the grey card, L_m is the measured luminance value of the grey card, L_d is the average derived luminance value of the grey card, $\sigma(L_d)$ is the absolute percentage standard deviation with respect to L_d, L_{sc} is the average luminance value of the scene, P_{card} is the percentage luminance value of the grey card with respect to the average luminance value of the scene, d is the distance between the grey card and the camera, $\sigma(L_{sc})$ is the dynamic range of the scene, L_r is the luminance ratio, E_m is the measured illuminance value of the scene, E_d is the derived illuminance value of the scene, and e is the error of the luminance map.

For $\sigma(L_d)$, the maximum value along both campaigns is 49.67% and has an associated e=103%, while the minimum value of 1.61% has an associated e= 16%. The data shows a tendency suggesting that low values of $\sigma(L_d)$ could be related to low values in the error e. Next, from both campaigns, the maximum average luminance value of the card is 571.82 $[\frac{cd}{m2}]$ and the minimum value is 42.13 $[\frac{cd}{m2}]$, however no defined correlation is observed between the L_{sc} values of the scene and e. Then, for P_{card}, its maximum value is 12.31%, and its minimum value is 0.52%. A slightly correlation between the P_{card} values and e is found, and suggests that higher P_{card} values can be associated with low e values. For the distance values d, the maximum distance is of 4 m, while the minimum distance is of 0.5 m, it is believed that d has a direct impact on the luminance values of the grey card, which is the parameter that shows a correlation with e. Then, the maximum value for $\sigma(L_{sc})$ is 3168.60 $[\frac{cd}{m2}]$, and the minimum value is 690.14 $[\frac{cd}{m2}]$. Here a more defined relationship with e is observed, where high $\sigma(L_{sc})$ values are correlated with high e values. Finally, the maximum value of L_r is 5, and the minimum value is 1.61, but no correlation is observed between the value of L_r and e. As the values of the parameters P_{card}, $\sigma(L_d)$ and $\sigma(L_{sc})$ show a correlation with the error e, each of these parameters and its correlation with e is plotted to further analyse their contribution to the error in the luminance maps.

5.2 Analysis of results

From the results it is observed that the error of all the luminance maps is positive, meaning the luminance values from the luminance maps are being overestimated. It is also observed that from the six luminance maps acquired during the first campaign, only two of them (Scene 5 and Scene 6) are valid, as they have an error below 25%. Next, from the luminance maps of the second campaign for Scene 3, only two out of six have an error below 25%, i.e. when the grey card is in position 2 and position 5. Finally, the second campaign for Scene 6 has the most valid maps, as five out of six have an error below 25%.

After reviewing the results from both campaigns shown in Table 5.2, the contribution of the different parameters to the error of the luminance maps is evaluated. From this evaluation, the parameters that are found to show correlation with the error of the luminance maps are: The percentage luminance value of the grey card concerning the average luminance value of the scene P_{card}, the uniformity of the luminance values along with the grey card $\sigma(L_d)$, and the dynamic range of the scene $\sigma(L_{sc})$. The relationship between each of these parameters and the error of the luminance maps is plotted on the graphs shown in Figure 5.8, Figure 5.9, and Figure 5.10 respectively. These graphs do not show the results of the luminance map with $e = 103\%$. All the points in the graphs below the line of 25% error (e), are valid luminance maps.

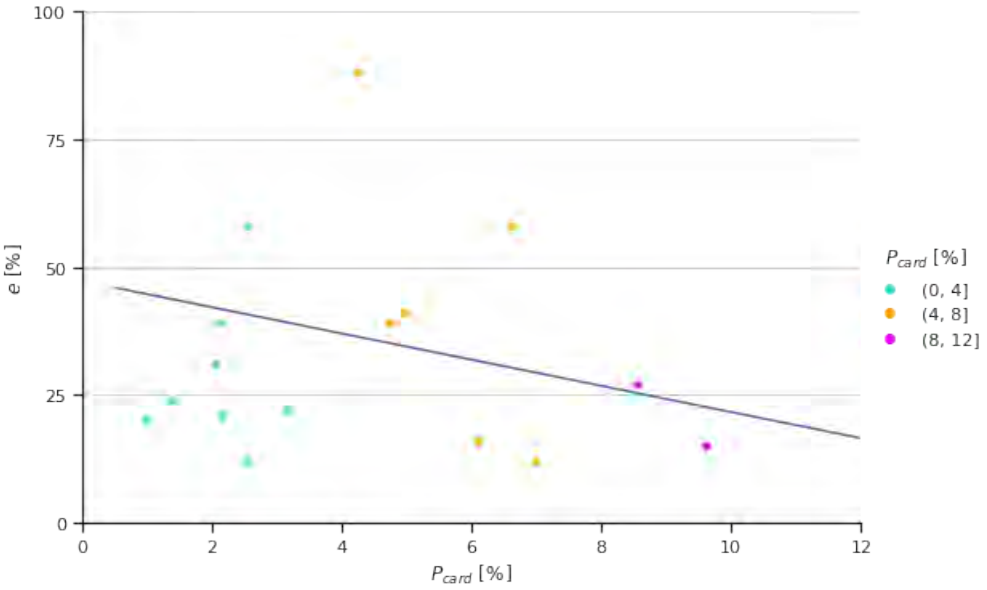

Figure 5.8: Graph showing the relationship between the percentage luminance value of the grey card with respect to the average luminance value of the scene (P_{card}), and the error (e).

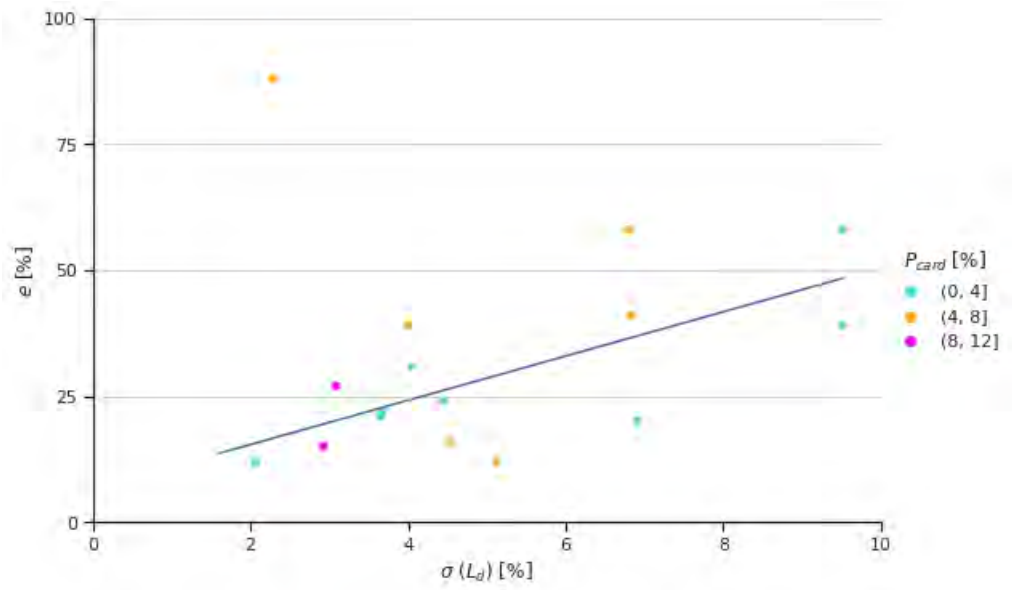

Figure 5.9: Graph showing the relationship between the percentage standard deviation of the grey card with respect to the derived average luminance value of the grey card $\sigma(L_d)$, and the error of the luminance maps (e).

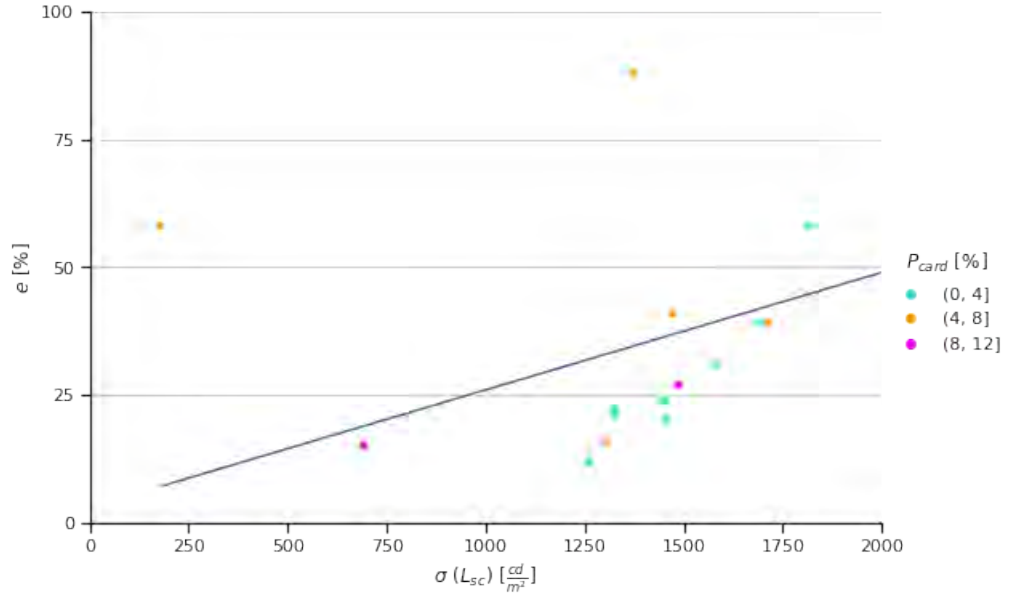

Figure 5.10: Graph showing the relationship between the standard deviation luminance of the scene $\sigma(L_{sc})$, and the error of the luminance maps (e). Values corresponding to valid luminance maps are identified with green, while the red ones are the ones from non valid luminance maps.

Figure 5.8 shows the relationship between the percentage luminance value of the grey card with respect to the average luminance value of the scene (P_{card}), and the error (e), where the data is classified into three categories depending on its P_{card} value. Light blue corresponds to P_{card} values ranging from 0% to 4%, orange corresponds to P_{card} values between 4% and 8%, and pink corresponds to P_{card} values from 8% to 12%. The data are grouped like this to easily visualize the trend and to correlate the P_{card} values with the $\sigma(L_d)$ of the grey card in Figure 5.9. In the graph of Figure 5.8, despite the dispersion in some values, the trend shows a decrease in the luminance map error when the percentage luminance values of the grey card are higher with respect to the average luminance from

the scene (P_{card}), which means that effectively placing the card somewhere in the scene with mid-range luminance values could decrease the error of the derived luminance maps. Then, from the graph in Figure 5.9, it is observed that the error of the luminance maps tends to increase as the percentage standard deviation of the luminance values with respect to the average luminance value of the grey card ($\sigma(L_d)$) increases, which means that keeping the uniformity of the luminance values along the grey card could contribute to reducing the error of the luminance maps. Each point on the graph shown in Figure 5.9 is colored depending on its P_{card} value, which despite the dispersion of some data, suggests a trend that higher luminance values in the grey card (P_{card}) are associated with a higher uniformity of the luminance values along with the grey card ($\sigma(L_d)$), especially for those points where the P_{card} value is between 0% and 4% . Finally, the graph of Figure 5.10 shows the percentage standard deviation of the luminance values of the scene and the error of the luminance maps. A higher standard deviation in the luminance values of the scene means that the dynamic range of the scene ($\sigma(L_{sc})$) is higher as well. From the graph it is observed that the higher the dynamic range of the scene, the higher the error of the luminance maps is likely to increase, which supports the findings of [22].

Although more data is needed to completely validate these hypotheses, the trend of the three different graphs points out that the error of the luminance maps is likely to be reduced if luminance along the grey card is kept uniform, and if the grey card is effectively placed somewhere in the scene with mid-range luminance values, as recommended by [22]. Additionally, as shown by Figure 5.10, it is observed that scenes with lower dynamic range will have more accurate luminance maps. Following the previous recommendations and the calibration and generation steps from Chapter 3 and Chapter 4, the acquired luminance maps should have less than 25% error in order to be useful to evaluate the luminance of a scene.

5.3 Luminance evaluations

Luminance maps can be used to perform different calculations. In this section the luminance maps with the best results from the first campaign shown of 5.1, which are Scene 5 and Scene 6, with 16% and 15% error, respectively, will be used to check if there are any glare sources in the scene and calculate the daylight glare probability (DGP).

The glare sources identified within the scene are shown in Figure 5.11. In table 5.3 the DGP value of each scene is presented, along with the number of glare sources found, their position (x,y), and their size in pixels. As mentioned in section 4.3, each glare source identified on the scene is marked with a different color, however, the color itself lacks any meaning. From the results in Table 5.3, all of the scenes have a DGP lower than 0.352, which according to Table 2.1 corresponds to an imperceptible glare.

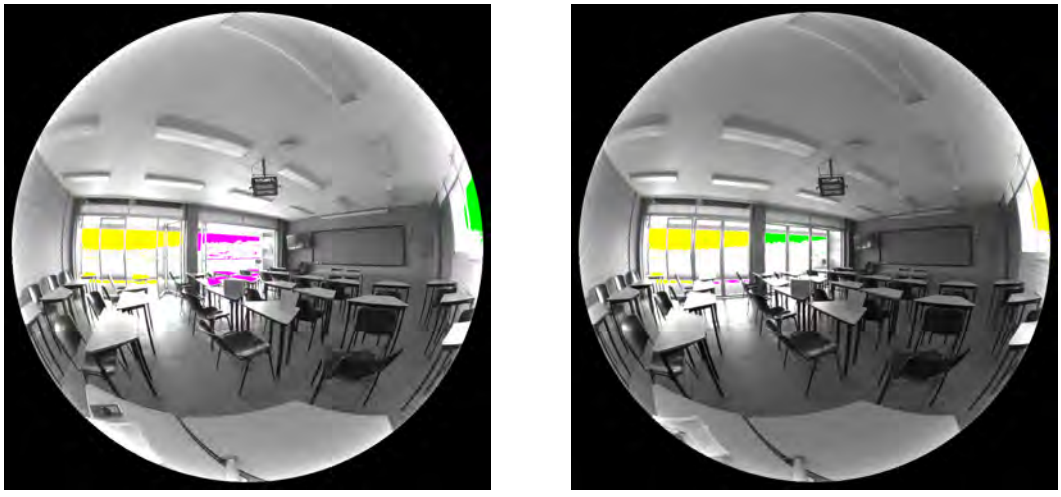

(a) Scene 5 (b) Scene 6

Figure 5.11: Glare sources in different colors identified for (a) Scene 5 and (b) Scene 6 of Campaign 1.

Apart from identifying and calculating the DGP of a scene, a mask can be made to the luminance map to identify an specific zone of the scene and retrieve its luminance values, as mentioned in section 4.3. In this thesis, an example of how to analyze the luminance values of an specific zone of a scene is presented. The Scene 1 from the

Sc [-]	Glare sources [-]	x [-]	y [-]	Size [pixels]	DGP
5	Source 1	255	495	8,205	0.29
	Source 2	458	513	3,136	
	Source 3	963	421	2,461	
6	Source 1	254	489	7,368	0.27
	Source 2	327	571	158	
	Source 3	448	482	1,498	
	Source 4	463	556	151	
	Source 5	963	420	2,497	

Table 5.3: Glare sources found for the scenes of the first campaign with lower error, as shown in table 5.2.

first campaign is selected to carry out this analysis. The area to be analysed is highlighted in a blue circle as shown in Figure 5.12, and corresponds to a part of a blackboard. The masking of the calibrated HDR image is done by following the steps of section 4.3. The average (L_{av}), the minimum (L_{min}), and maximum luminance of this area (L_{max}), along with the standard deviation of luminance (σ(L)) are derived and shown in Table 5.4.

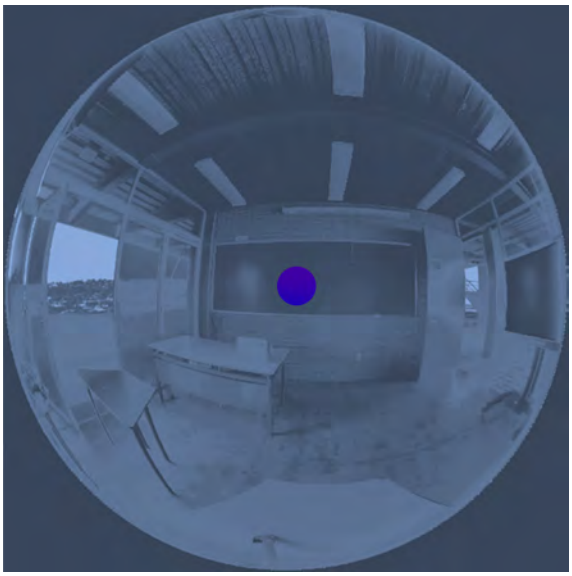

Figure 5.12: Luminance of an specific part of the Scene 1.

Size [pixels]	L_{av} $[\frac{cd}{m2}]$	L_{min} $[\frac{cd}{m2}]$	L_{max} $[\frac{cd}{m2}]$	$\sigma(L)$ $[\frac{cd}{m2}]$
12,849	8.33	6.24	11.12	1.15

Table 5.4: Retrieved luminance values for an specific zone of the luminance map from Scene 1.

The average luminance of this specific part of the scene is within the range of luminance values indicated by the color scale in the map from Scene 1, which is shown in Figure 5.4 (a) Scene 1. The analysed area corresponds to the center part of the blackboard in Scene 1, which has low luminance indicated by purple color. Any other area of the scene can be analyzed doing the corresponding mask by following the steps of section 4.3. Addittionaly, knowing the luminance of the scene, the illuminance values can also be derived, if the reflectance value of the area to be analysed is known using the following equation:

$$L = E \times p \tag{5.3}$$

where L is the luminance value, E corresponds to the illuminance value, and p corresponds to the reflectance value.

CHAPTER 6

Conclusions

Luminance maps are a valuable tool to evaluate lighting conditions within a scene. During this thesis, a method to acquire accurate luminance maps with commercial equipment and intermediate coding skills is done and presented, based on the procedure defined in [22]. During the experimental campaigns, the importance of deriving an accurate luminance ratio to photometrically calibrate a high dynamic range (HDR) image and derive a luminance map is discussed. The results from the campaigns show that scenes with a low dynamic range; (i.e, having more uniform luminance values along with the scene), will result in more accurate luminance maps. Additionally, keeping the luminance values along with the grey card uniform, by effectively placing the card somewhere in the scene with mid-range luminance values, can enhance the accuracy of the maps derived. As stated in [22], it is expected that scenes that have a wide luminance range are prone to high errors, which is the case for Scene 3. This can be appreciated in the luminance maps shown in 5.4, where the map from Scene 6 have a more homogeneous luminance than that from Scene 3. Additionally, in [22] it is stated that, in general, the error between the measured and derived illuminance values should be expected to be lower than 10%. In this work, the lowest error in the luminance maps is obtained during the second campaign for Scene 6, when the grey card is in positions 4 and 6, which gives an error of 12%, as shown in Table 5.2. It is believed that the error of the luminance maps can be further reduced by following the recommendations proposed in section 5.2 of this work.

After addressing the encountered problems during the calibration of the high dynamic range images to acquire luminance maps, and taking into account the error that could be added by the measuring equipments, accurate luminance maps can be obtained following the steps described in this thesis. Additionally, it is observed that the luminance maps are useful to perform glare analysis within a scene and evaluate the probability of discomfort. Furthermore, the luminance maps can be modified to obtain the luminance values of delimited areas within a scene, and by knowing the reflectance value of the different surfaces, the illuminance values could be derived as well.

The process to obtain luminance maps with the Canon 6D EOS mark II is automated in Bash, from remotely controlling the camera to take the low dynamic range (LDR) images with different exposure values, to calibrating and acquiring a luminance map. The script of the automated process is shown in the Appendix B. It is also desirable to continuously generate luminance maps during long periods of time to evaluate the conditions in different scenes, therefore the process described during this thesis is also automated for a Raspberry Pi working with a Pi Camera module v2 and an attached fisheye lens. Due to the restrictions of the Covid-19 pandemic, it was not possible to calibrate the fisheye lens attached to the Raspberry Pi camera module, and as the lens lacks of documentation, the projection type of the fisheye lens is unknown, hence the real angle of view cannot be derived. However, the automation process is done for the Rasberry Pi to take pictures with different exposure values, merge them and generate high dynamic range images that can be further calibrated in the same script to acquire luminance maps. The script to do this is shown in C. It is expected that after the calibration of the fisheye lens and derivation of the luminance ratio for the HDR image to be calibrated, accurate luminance maps with errors under 25% can be obtained. The Raspberry Pi is to be implemented in the different classrooms for the project "Demonstrative buildings of bioclimatic design in a warm sub-humid climate at the Renewable Energy Institute - UNAM", to continuously evaluate the luminance conditions. Although no glare analysis will be done using the Raspberry Pi due to its fixed positions in the classrooms, the automated process using the Canon 6D EOS mark II is aimed to carry out experimental campaigns in different scenes to evaluate glare and discomfort.

It should be addressed that knowing the reflectance of the different materials in the scene would allow luminance maps to be transformed into illuminance maps, leading to a more complete evaluation of the lighting conditions within a scene. Furthermore, machine learning algorithm could be implemented in the automated processes for

both the Canon 6D EOS mark II and the Raspberry Pi devices to identify specific zones in the scene and retrieve its luminance and illuminance values. This could lead to derive accurate luminance ratios for the photometric calibration of the HDR images without needing a luminance meter, which would further reduce the costs of these processes. This could also enable the process to detect specific areas of interest within a scene and automatically derive the luminance and illuminance value of those areas while identifying glare sources and evaluating visual comfort.

Finally, the repository in https://github.com/Mary-Lo/HDR contains the scripts used to calibrate the camera lens, the Python codes needed to calibrate the HDR images, as well as the scripts of the complete automated process to acquire accurate luminance maps for both the Canon EOS 6D Mark II, with an attached Sigma 8mm F3.5 EX DG Fisheye lens, and the Raspberry Pi, with the Camera Module V2 and attached MakerFocus fisheye lens.

APPENDIX A

Hardware and software

In this appendix, the complete list of hardware and software used during this thesis to acquire luminance maps are listed.

A.1 Hardware

- **Canon EOS 6D Mark II**

  It has a CMOS sensor of 26.2 MP and is used during this work to take the low dynamic range pictures (LDR) with different exposure values.

- **Sigma 8mm F3.5 EX DG Fisheye lens**

  This circular fisheye lens is attached to the Canon EOS 6D Mark II, it has an equidistant projection and produces circular images.

- **Neewer® 200mm Professional Rail Nodal Slide**

- **Neewer® PU-50 universal plate**

- **Neewer® 18% Gray Card 8" x 10"**

- **Vanguard VT-118 tripod**

- **Konica Minolta Illuminance Meter T-10A**

  This illuminance meter is set during this thesis to the measuring function of average illuminance in lux. It has a linearity of 2% ± 1 digit of value display.

- **Konica Minolta Luminance meter LS-160**

  This luminance meter has a measuring angle of 0.3 degrees. During this thesis it is used without a close-up lens, therefore the shortest distance for measurement is 1.012 m. This luminance meter has an accuracy of ± 2% ± 2 digits which corresponds to 10 $\frac{cd}{m^2}$ or less.

- **Raspberry Pi 3B+** The process to generate luminance maps from LDR images is automated for the Raspberry Pi3B+, and will be used to continuously monitor luminance conditions in the classrooms.

- **Camera Module V2** The camera module V2 is connected to the Raspberry Pi 3B+.

- **MakerFocus fisheye lens** This fisheye lens is attached to the camera module V2.

A.2 Software

The following open software are installed in a computer that runs under the Ubuntu 20.04 operating system.

- **RawTherapee**

  Open software to process photographs. It is used in this work to process and visualize the RAW pictures captured with the Canon 6D EOS mark II.

- **qDslrDashboard**

  Open software that allows to remotely control different digital cameras through an interface. In this thesis the software is used to control the Canon 6D EOS mark II, set the camera settings and configure the bracketing process.

- **Radiance**

  An open source suite of tools to perform lightning simulations. In this thesis the Radiance tools utilized to generate, calibrate and analyze luminance maps are: raw2hdr, ra_xyze, pcompos, pcomb, pvalue, evalglare and falsecolor.

- **gphoto2**

  Open software implemented in the automation process to remotely control the Canon 6D EOS mark II, as it allows to configure camera settings and bracketing from the UNIX terminal.

APPENDIX B

Automation code for the Canon 6D EOS mark II

```
#!/bin/bash

DATE=$(date +"%m_%d_%Y")

## FIX CAMERA SETTINGS FOR THE BRACKETING

sudo gphoto2 --set-config=/main/imgsettings/iso=100
sudo gphoto2 --set-config=/main/imgsettings/whitebalance=2
sudo gphoto2 --set-config=/main/imgsettings/imageformat=28
sudo gphoto2 --set-config=/main/capturesettings/aperture=11
sudo gphoto2 --set-config=/main/imgsettings/colorspace=0
sudo gphoto2 --set-config=/main/


## BRACKETTING

sudo gphoto2 --set-config=/main/capturesettings/shutterspeed=1/4000
--capture-image-and-download --filename=raw1.cr2
sudo gphoto2 --set-config=/main/capturesettings/shutterspeed=1/3200
--capture-image-and-download --filename=raw2.cr2
sudo gphoto2 --set-config=/main/capturesettings/shutterspeed=1/1600
--capture-image-and-download --filename=raw3.cr2
sudo gphoto2 --set-config=/main/capturesettings/shutterspeed=1/800
--capture-image-and-download --filename=raw4.cr2
sudo gphoto2 --set-config=/main/capturesettings/shutterspeed=1/400
--capture-image-and-download --filename=raw5.cr2
sudo gphoto2 --set-config=/main/capturesettings/shutterspeed=1/200
--capture-image-and-download --filename=raw6.cr2
sudo gphoto2 --set-config=/main/capturesettings/shutterspeed=1/100
--capture-image-and-download --filename=raw7.cr2
sudo gphoto2 --set-config=/main/capturesettings/shutterspeed=1/50
--capture-image-and-download --filename=raw8.cr2
sudo gphoto2 --set-config=/main/capturesettings/shutterspeed=1/25
--capture-image-and-download --filename=raw9.cr2
sudo gphoto2 --set-config=/main/capturesettings/shutterspeed=1/13
--capture-image-and-download --filename=raw10.cr2
sudo gphoto2 --set-config=/main/capturesettings/shutterspeed=1/6
--capture-image-and-download --filename=raw11.cr2
```

```
sudo gphoto2 --set-config=/main/capturesettings/shutterspeed=0.3
--capture-image-and-download --filename=raw12.cr2
sudo gphoto2 --set-config=/main/capturesettings/shutterspeed=0.6
--capture-image-and-download --filename=raw13.cr2
sudo gphoto2 --set-config=/main/capturesettings/shutterspeed=1.3
--capture-image-and-download --filename=raw14.cr2

## RUN PYTHON SCRIPT FOR THE DARKEST AND BRIGHTEST EXPOSURE TO CHECK
IF THE IMAGES COVER THE WHOLE DYNAMIC RANGE OF THE SCENE

py=$(python3 python_EV.py)

if [[ $py -eq 0 ]]
then
  echo "True"
else
  echo "False"
  #Combine LDR images
  raw2hdr -a -e -f -g -h -w -o image.hdr *.cr2

  #Nullificate exposure value
  ra_xyze -r -o image.hdr > image_nullEV.hdr

  #View image and select grey card
  echo "Select two corners of the grey card and give me the coordinates x and y"
  ximage image_nullEV.hdr

  echo"So..the coordinates of the first point are:"
  echo "x1"
  read x1
  echo "y1"
  read y1
  echo "And the coordinates of the second point are:"
  echo "x2"
  read x2
  echo "y2"
  read y2

  sizex=$((x2-x1))
  sizey=$((y2-y1))

  #Crop the image to just select the grey card
  pcompos -x $sizex -y $sizey image_nullEV.hdr -$x1 -$y1 >image_crop.hdr

  #Obtain RGB values of image
  pvalue -h -H -d image_crop.hdr > grey.csv

  #Run python script to obtain average luminance
  b=$(python3 gray_mean.py)
```

```
  echo "The average luminance is $b"

  echo "What is the luminance measure from luminometer?"
  read luminance

  c=$(echo "$b/$luminance"|bc -l)

  echo "The luminance ratio is: $c"

  #Crop fisheye image for the analysis
  pcompos -x 2060 -y 2060 image_nullEV.hdr -550 -10 > crop.hdr

  ##Resize image
  pfilt -1 -x 1000 -y 1000 crop.hdr > image_resize.hdr

  ##Add vignetting function
  pcomb -f vignetting.cal image_resize.hdr > image_vignetting.hdr

  ##Make photometric adjustment
  pcomb -s $c image_vignetting.hdr > image_photometric.hdr

  ##Change view angle for fisheye
  getinfo -a "VIEW= -vta -vv 186 -vh 186" < image_photometric.hdr > image_final.hdr

  ##Print illuminance value
  echo "Total illuminance is:"

  evalglare -V image_final.hdr
  evalglare -V image_final.hdr > illuminance.txt

  ##Crop to a 180 degree view
  pcomb -e 'Cx:xmax/2;Cy:ymax/2;R:600;sq(x):x*x' -e 'inC=sq(R)-sq(x-Cx)-sq(y-Cy)'
  -e 'ro=if(inC,ri(1),0);go=if(inC,gi(1),0);bo=if(inC,bi(1),0)'
  -o image_final.hdr > adjust_180.hdr

  ##Make the luminance map
  falsecolor -s 5000 -d 1  -i adjust_180.hdr -log 3 > image_map.hdr
fi
```

APPENDIX C

Automation code for the Raspberry Pi

```
#!/bin/bash

DATE=$(date +"%Y-%m-%d_%H%M")

#raspistill -o /home/pi/Documents/$DATE.jpg

raspistill -n -r -ISO 100 -awb sun -t 500 -ss 100 -o 1.jpg
raspistill -n -r -ISO 100 -awb sun -t 500 -ss 500 -o 2.jpg
raspistill -n -r -ISO 100 -awb sun -t 500 -ss 1000 -o 3.jpg
raspistill -n -r -ISO 100 -awb sun -t 500 -ss 5000 -o 4.jpg
raspistill -n -r -ISO 100 -awb sun -t 500 -ss 10000 -o 5.jpg
raspistill -n -r -ISO 100 -awb sun -t 500 -ss 50000 -o 6.jpg
raspistill -n -r -ISO 100 -awb sun -t 500 -ss 100000 -o 7.jpg
raspistill -n -r -ISO 100 -awb sun -t 500 -ss 500000 -o 8.jpg
raspistill -n -r -ISO 100 -awb sun -t 500 -ss 1000000 -o 9.jpg
raspistill -n -r -ISO 100 -awb sun -t 500 -ss 2000000 -o 10.jpg

python3 PyDNG/examples/utility.py 1.jpg
python3 PyDNG/examples/utility.py 2.jpg
python3 PyDNG/examples/utility.py 3.jpg
python3 PyDNG/examples/utility.py 4.jpg
python3 PyDNG/examples/utility.py 5.jpg
python3 PyDNG/examples/utility.py 6.jpg
python3 PyDNG/examples/utility.py 7.jpg
python3 PyDNG/examples/utility.py 8.jpg
python3 PyDNG/examples/utility.py 9.jpg
python3 PyDNG/examples/utility.py 10.jpg

raw2hdr -a -e -g -f -h -w -o im.hdr *.dng

#Get info about the final HDR
getinfo im.hdr

#Nullificate exposure value
ra_xyze -r -o im.hdr > image_nullEV.hdr

#Crop image (not cropping for the fisheye of this raspberry)
```

```
#pcompos -x 2060 -y 2060 image_nullEV.hdr -550 -10 > crop.hdr

#Resize image
pfilt -1 -x 1000 -y 1000 image_nullEV.hdr > image_resize.hdr


#Make photometric adjustment
pcomb -s 1.8 image_resize.hdr > image_photometric.hdr

#Change view angle for fisheye
getinfo -a "VIEW= -vta -vv 121 -vh 121" < image_photometric.hdr > image_final.hdr

#Print illuminance value
echo "Total illuminance is: "

evalglare -V image_final.hdr

evalglare -V image_final.hdr > illuminance.txt

mv image_final.hdr HDR_images/$DATE.hdr

rclone copy --update --verbose --transfers 5 --checkers 2 --contimeout 60s
--timeout 300s --retries 3 --low-level-retries 5 --stats 1s
"/home/pi/Desktop/Picture_Apolo_1/HDR_images" "HDR: drive"
```

Bibliography

[1] Admesy. *Does the Human Eye Perceive Light? Photopic and Scotopic Vision.* 2020. URL: https://www.azom.com/article.aspx?ArticleID=14971.

[2] International Energy Agency. '25 energy efficiency policy recommendations'. IEA Paris. 2011.

[3] J. Alstan et al. 'Accurate measurement of daylit interior scenes using high dynamic range photography'. *Proceedings of the CIE 2016 Lighting Quality and Energy Efficiency Conference*. 2016.

[4] C. Bilu et al. 'Beneficial effects of daytime high-intensity light exposure on daily rhythms, metabolic state and affect'. *Scientific reports* 10.1 (2020), p. 1.

[5] D. Bowskill. *The complete guide to photography*. First Edition. COLES, 1980.

[6] S. Carlucci et al. 'A review of indices for assessing visual comfort with a view to their use in optimization processes to support building integrated design'. *Renewable and sustainable energy reviews* 47 (2015), pp. 1016–1033.

[7] C. Cauwerts, M. Bodart and D. Arnaud. 'Comparison of the vignetting effects of two identical fisheye lenses'. *Leukos* 8.3 (2012), p. 181.

[8] N. Chauhan and B. Choi. 'Performance analysis of denoising algorithms for human brain image'. *International Journal of Fuzzy Logic and Intelligent Systems* 18.3 (2018), p. 175.

[9] A. Choudhury. *Principles of colour and appearance measurement: Object appearance, colour perception and instrumental measurement*. Elsevier, 2014.

[10] S. Cox. *What is exposure?(A Beginner's guide)*. 2020. URL: https://photographylife.com/what-is-exposure.

[11] P. Debevec and J. Malik. 'Recovering high dynamic range radiance maps from photographs'. *ACM SIGGRAPH 2008 classes*. 2008.

[12] M. Grossberg and S. Nayar. 'What is the space of camera response functions?' *2003 IEEE Computer Society Conference on Computer Vision and Pattern Recognition, 2003. Proceedings.* Vol. 2. IEEE. 2003, p. 602.

[13] M. Inanici. 'Evaluation of high dynamic range photography as a luminance data acquisition system'. *Lighting Research and Technology* 38.2 (2006), p. 123. DOI: 10.1191/1365782806li164oa.

[14] J. Jakubiec et al. 'Accurate measurement of daylit interior scenes using high dynamic range photography'. *Proceedings of the CIE 2016 Lighting Quality and Energy Efficiency Conference*. 2016.

[15] J. Kidger. *Fundamental Optical Design*. 2020. URL: https://spie.org/publications/pm92_161_marginal_chief_rays?SSO=1.

[16] N. Klepeis et al. 'The National Human Activity Pattern Survey (NHAPS): a resource for assessing exposure to environmental pollutants'. *Journal of Exposure Science & Environmental Epidemiology* 11.3 (2001), p. 231.

[17] K. Konis and S. Selkowitz. *Effective daylighting with high-performance facades: emerging design practices*. Springer, 2017.

[18] J. Lambert and A. Edwards. *Electromagnetic Radiation*. 2020. URL: http://www.ces.fau.edu/nasa/module-2/radiation-sun.php.

[19] S. McHugh. *Cameras vs the human eye*. 2020. URL: https://www.cambridgeincolour.com/tutorials/cameras-vs-human-eye.htm.

[20] Nikon. *DSLR Camera Basics*. 2020. URL: https://imaging.nikon.com/lineup/dslr/basics/13/index.htm.

[21] C. Pierson, J. Wienold and M. Bodart. 'Daylight discomfort glare evaluation with Evalglare: influence of parameters and methods on the accuracy of discomfort glare prediction'. *Buildings* 8.8 (2018), p. 94.

[22] C. Pierson et al. 'Tutorial: Luminance Maps for Daylighting Studies from High Dynamic Range Photography'. *LEUKOS* (2020), p. 31. DOI: 10.1080/15502724.2019.1684319.

[23] E. Reinhard et al. *High dynamic range imaging: acquisition, display, and image-based lighting*. Morgan Kaufmann, 2010.

[24] N. Ruck et al. 'Daylight in Buildings-A source book on daylighting systems and components'. *Lawrence Berkeley National Laboratory* (2000), p. 9910.

[25] J. Smith. *Modern Optical Engineering: the design of optical systems*. Fourth Edition. McGraw-Hill Professional, 2007.

[26] J. Wienold. 'Dynamic daylight glare evaluation'. *Proceedings of Building Simulation*. 2009, p. 944.

[27] J. Wienold and J. Christoffersen. 'Evaluation methods and development of a new glare prediction model for daylight environments with the use of CCD cameras'. *Energy and buildings* 38.7 (2006), p. 743.

[28] Wikipedia. *Bayer filter*. 2021. URL: https://en.wikipedia.org/wiki/Bayer_filter.

[29] D. Wüller and H. Gabele. 'The usage of digital cameras as luminance meters'. *Digital Photography III*. Vol. 6502. International Society for Optics and Photonics. 2007, p. 65.

[30] H. Xiao, H. Cai and X. Li. 'Non-visual effects of indoor light environment on humans: A review'. *Physiology & Behavior* (2020), p. 113195.

[31] V. Zaikina. 'Light modelling in architectural spaces: Luminance-bases metrics of contour, shape and detail distinctness of day-lit 3D objects'. *NTNU* (2016).